# Determining Tumor Blood Flow Parameters Using Dynamic Imaging Data

by

Jessica Meade Libertini

B.S., Johns Hopkins University, Baltimore, MD, 1999

Sc.M., Brown University, Providence, RI, 2003

M.S., Rensselaer Polytechnic Institute, Troy, NY, 2004

A dissertation submitted in partial fulfillment of the
requirements for the degree of Doctor of Philosophy
in the Division of Applied Mathematics at Brown University

PROVIDENCE, RHODE ISLAND

May 2008

Abstract of "Determining Tumor Blood Flow Parameters Using Dynamic Imaging Data," by Jessica Meade Libertini, Ph.D., Brown University, May 2008

This thesis discusses two different topics, both related to the goal of determining tumor blood flow parameters from time-sequenced contrast-enhanced medical image data in an effort to quickly measure the efficacy of cancer treatments. This work builds upon existing work in the radiology field by using a commonly accepted two-compartment model. In this model, the blood flow parameters are represented as four constant coefficients: the perfusion, the permeability surface area product, and the relative volumes of each of the two compartments. For the purposes of the testing the ideas presented in this thesis, computational baseline data is used; although not actual patient data, this baseline was developed to emulate real patient data.

The first major topic is a parametric study. Since the application of this work is in the form of an inverse problem, i.e., the coefficients are the unknowns, it is important to understand the roles of each of the four coefficients with respect to their impact on the overall signal intensity of the medical images. Therefore, a set of numerical experiments was designed and executed to clarify the relationships each of the four coefficients has with the signal intensity. The results of these experiments are presented along with a discussion of how the numerical results relate to the physiological system being modeled.

The second major topic has two parts. In the first part, questions are raised and explored involving the validity of a model simplification in the existing literature. The second part proposes new methods for computing two of the coefficients; these alternative methods do not require the use of the simplification in question. This simplification arises from a difficulty in measuring the time-dependent outflow of contrast agent leaving the capillary via the venule. The assumption leading to this

simplification is explored, and the existence of the error is verified through calculations. The beginning stages of alternative methods that do not require the use of the erroneous simplification are also presented. In this work, two of the four coefficients are recovered with high accuracy through numerical experiments. A method for determining the missing boundary condition is also presented. To demonstrate the robustness of these methods in the presence of low image frequency, only subsets of baseline analytical data are passed as input to the computations.

This dissertation by Jessica Meade Libertini is accepted in its present form by the Division of Applied Mathematics as satisfying the dissertation requirement for the degree of Doctor of Philosophy.

Date_____ _____

David Gottlieb, Ph.D., Advisor

Recommended to the Graduate Council

Date_____ _____

Wai Sun Don, Ph.D., Reader

Date_____ _____

Chi-Wang Shu, Ph.D., Reader

Approved by the Graduate Council

Date_____ _____

Sheila Bonde, Dean of the Graduate School

The Vita of Jessica Meade Libertini

Born on December 11, 1977 in Baltimore, Maryland, USA.

## Education

- M.S. in Mechanical Engineering, Rensselaer Polytechnic Institute, Troy, New York, August, 2004.
- Sc.M. in Applied Mathematics, Brown University, Providence, Rhode Island, May 2003.
- B.S. in Mechanical Engineering, Johns Hopkins University, Baltimore, Maryland, May 1999.

## Publications/Preprints

- J. Libertini, *Determining Tumor Blood Flow Parameters from Dynamics Image Measurements*, Journal of Physics: Conference Series, to appear.

## Research Interests

- Mathematical Modeling.
- Numerical Methods.
- Medical Imaging and Physiological Modeling.
- Fluid Dynamics.
- Systems Engineering.

## Academic and Professional Experience

- Senior Engineer and System Analyst: General Dynamics, January 2003 - September 2004 *and* July 2007 – Present.
- Research Assistant: Division of Applied Mathematics, Brown University, January 2002 – January 2003 *and* September 2004 – July 2007.
- Teaching Fellow: *Analytic Geometry and Calculus*, Mathematics Department, Brown University, Fall Semester 2006.
- Adjunct Faculty: Department of Mathematics, Three Rivers Community College, January 2001 – December 2007, intermittent.
- Systems Engineer: General Dynamics, July 1999 – January 2002.
- Research Assistant: Department of Mechanical Engineering, Johns Hopkins University, May 1996 – May 1999.

## Synergistic Activities and Service

- Charter Member: Rose Whelan Society for Women in Mathematics, Brown University.
- Summer Engineering Instructor: Center for Talented Youth, Johns Hopkins University, July 2006.
- Invited Panelist: Women in Mathematics Career Panel, Brown University, April 2004.
- Director of Outreach Programs: Society of Women Engineers, Johns Hopkins University, September 1997 – May 1999.

## Awards and Honors

- VIGRE Fellowship, 2004-2005, Brown University.
- Dean Fellowship, 2002-2003, Brown University.
- Baxley Scholarship for Undergraduate Engineers, 1995-1997, Johns Hopkins University.
- Schrivner Scholarship, 1995, Johns Hopkins University.

**Acknowledgments**

First and foremost, I want to express my deepest gratitude to my advisor, Professor David Gottlieb, for his invaluable wisdom and guidance, unwaivering support, and unconditional encouragement throughout my graduate career at Brown University. I also wish to thank Professor Wai Sun Don, Professor Sidi Kaber, and Professor Chi-Wang Shu for helping me shape this work. I also owe my gratitude to Dr. Cédric deBazelaire, who has served as my professional liaison to the radiology community.

I also wish to acknowledge my current and former management at General Dynamics, Dr. Millard Firebaugh, Mr. Jack Morgan, Mr. Daniel Panosky, and Mr. Thomas Berry, for recognizing my aspirations and allowing me the time I needed to pursue my dreams.

I would like to thank the staff in the Division of Applied Mathematics and the Mathematics Department for their patience, their smiles, and their infinite wisdom on navigating administrative matters.

Many thanks are due to my dear friends and colleagues: Dr. Agnieszka Czopik for setting a shining example to follow, Dr. Alina Bucur for giving me her advice and support, and Mr. Sergey Kushnarev for adding so much joy to my life as a graduate student.

I wish to thank my family for their love and for teaching me to question, to study, and to discover: my parents, Ken & Nancy Libertini; my sister and her husband, Katie & Jim Bolyard; my grandparents, John & Harriet Libertini, Jack & Maggie Schoelkopf, and Tip & Nicky Quillen. And last, but certainly not least, I wish to thank Mr. Denis Mikhaylov, whose love and support made the completion of this dissertation possible.

# Contents

# List of Tables

# List of Figures

# Chapter 1

# Introduction

Cancer is one of the leading causes of death in the civilized world. Many new cancer treatments focus on reducing or eliminating angiogenesis, the process by which a tumor develops highly efficient capillary beds in support of the tumor's rapid growth. The standard procedure for measuring the efficacy of such treatments involves comparing the results of two contrast enhanced imaging tests, taken months apart. To determine if the tumor's growth has been sufficiently arrested by the treatment, the size of the contrast-enhanced regions of the static images are compared from one test to the next. The goal of this research is to reduce the time between tests from months to just weeks or even days by using all of the dynamic time data available from the imaging session to characterize the blood flow to the tumor. After a very brief introduction to the circulatory system, a more detailed description of angiogenesis is provided in Section 1.1. Section 1.2 explains current radiological practices for tumor identification and classification. Section 1.3 provides a brief overview of the following chapters.

## 1.1 Understanding Angiogenesis: An Introduction to the Physiology of Cancer Growth

The circulatory system provides the human body with its supply of oxygen and other metabolites using a tapered network of blood vessels. Oxygen-rich blood leaves the heart, and is carried to the rest of the body by a system of arteries. Starting from the aorta, the main arteries bifurcate, branching out to every part of the body and getting smaller in size. The smallest of these arteries are the arterioles which are slightly larger in diameter than a single red blood cell. Upon exiting an arteriole, oxygenated blood enters into a capillary. Capillaries are the smallest blood vessels in the body, and as the red blood cells squeeze through these tiny vessels, oxygen and metabolites leak out through the porous membrane of the capillary wall. The capillaries are the only blood vessels which allow transport across their walls. In addition to oxygen, other molecules can exit or enter the capillary via the capillary walls, and this transport is driven by both passive transport (osmotic pressure gradients) and active transport (biochemical forces). At the end of the capillary, blood enters the smallest of the veins, a venule. The small veins merge together to make larger and still larger veins until the blood is returned to the heart and lungs, and the process begins again [1].

With the exception of a developing fetus, cancerous tumors are the fastest growing entity in the adult human body. In order to maintain this growth rate, the tumor has a higher need for oxygen and other blood-delivered metabolites than the surrounding healthy tissue. To entice the local network of blood vessels to support its demands, the tumor mimics the body's natural mechanism for growing new capillary beds. When the body requires new microvascular structure, for example during the healing of a wound, the regenerating tissue emits VEGF, vascular endothelial growth factor. VEGF serves as the signal to the circulatory system to send more blood. VEGF is captured by special receptors on nearby arteries, and a new network of blood vessels

begins to grow towards the source of the VEGF. In healthy tissue, once the demand for blood is met, VEGF production is terminated, and the body stops growing new blood vessels.

To meet its ever increasing demands for more blood to support its rapid growth, a tumor releases VEGF and lures the circulatory system to feed the tumor with new vasculature, as illustrated in Figure 1.1. Unlike healthy tissue which will stop the growth process by ceasing the release of VEGF, as a tumor grows, it continues to release VEGF [2]. In addition to increasing the number of blood vessels in the tumorous region, the body responds to this constant demand by developing capillaries with a higher efficiency than those which feed healthy tissue. This higher efficiency is achieved by increasing the permeability of the capillary walls, thus allowing particles to cross the capillary membrane more freely. This means that in a tumorous region, the number of blood vessels is higher, the capillaries have a higher permeability, and the perfusion of blood is also increased relative to normal tissue [3]. By identifying these parameters, the degree of angiogenesis can be measured [4].

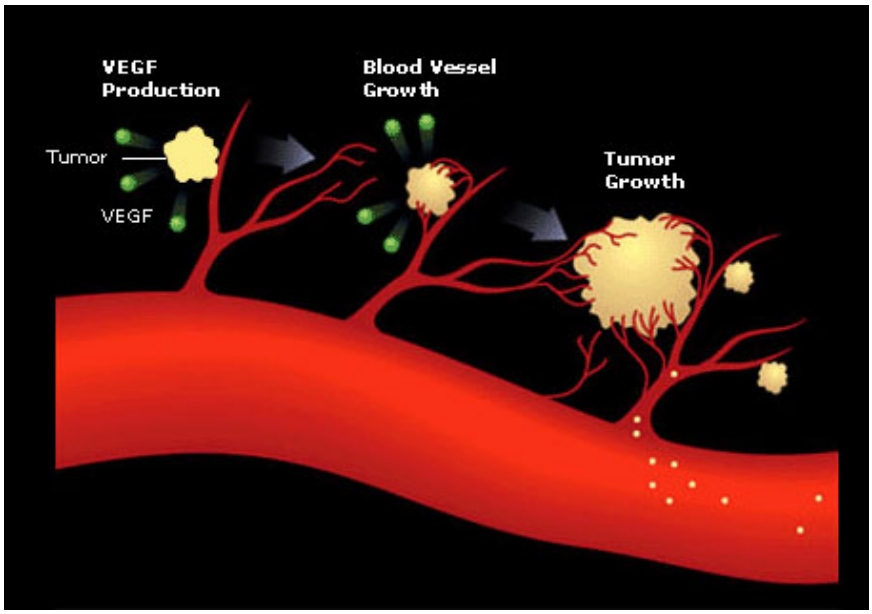


Figure 1.1: The release of VEGF entices nearby blood vessels to grow new blood vessels.

## 1.2 Current Radiological Techniques

Many cancer treatments work to inhibit angiogenesis in an effort prevent continued tumor growth [5]. While there is great promise in these treatments, not all treatments are effective for all patients. Therefore it is necessary to measure the efficacy of these treatments. Typically, upon the discovery and classification of a cancerous tumor, the patient undergoes a test involving either contrast-enhanced Magnetic Resonance Imaging (MRI) or contrast-enhanced Computerized Tomography (CT) [4, 5, 6]. In dynamic MRIs, a tracer with a relaxation time far different than any naturally occurring material in the body, typically gadolinium-diethylenetriamine penta-acetic acid (Gd-DTPA), is used. In dynamic CTs, the typical tracer is a nonionic iodinated contrast agent, such as iopromide. In either case, a contrast agent is injected into the patients bloodstream. Then a sequence of images in the region of interest captures the flow of the tracer. A radiologist looks at these images in a static sense and tries to estimate the size of the tumor. The difficulty is that while regions of angiogenesis will show up with a high concentration of the contrast agent, the rest of the surrounding tissue will also have some tracer. In practice, the size determination is often based on one image chosen out of the sequence. If the image chosen was too early in the sequence, the entire region of the tumor may not have been highlighted yet, thereby underestimating the size of the tumor. Conversely, if the image selected was too late in the sequence, the contrast agent would have had time to diffuse through the tumor region as well as seep into the healthy tissue fed by the healthy capillary beds. This would make it difficult to find the true edges of the tumor, perhaps resulting in overestimating the size. Upon the recommendation of the oncologist, the patient begins a treatment regiment, and after three to six months, the radiologist repeats the test. If the treatment is working, then the tumor will not have grown since the previous test. However, if the treatment is not working, the patient will have dealt with the devastating side effects of a treatment that has not helped, on top of losing six months of treatment time in his or her battle with cancer. Additionally, the

high financial cost of cancer treatments lends further justification to determine their efficacy in a timely fashion.

## 1.3 Overview

The remaining chapters of this thesis explore the concept of using all the dynamic imaging data available to characterize the blood flow to the tumor, thus determining the efficacy of the treatment in a much shorter time-scale than the method outlined above.

The original work in this thesis is built upon work by others, both in the mathematical field and in the radiology field, therefore it is important to understand this collective work. In Chapter 2, the problem of measuring tumor blood flow parameters from dynamic imaging data is presented in the context of this existing body of literature. While not an exhaustive representation of the work that has been done on this problem, Chapter 2 does highlight certain important results, including: defining the model; identifying the parameters; introducing the inverse problem and methods to solve it. Chapter 3 looks at the relationships between various terms in the model. Chapter 4 challenges a commonly accepted simplification to this model and presents alternative approaches to determining two of the blood flow parameters. After a short review of the work presented, Chapter 5 discusses some ongoing and future work related to this problem.

# Chapter 2

# Background

In an effort to make this thesis easily accessible and useful to interested members of the medical community, the new research presented is built upon a large body of existing research that has come from the radiology community. This chapter presents several key elements from the existing literature, supplying the reader with the necessary background to understand the work presented in this thesis as well as to understand its importance in the context of the field. Section 2.1 provides a brief overview of the proposed new approach for measuring the efficacy of cancer treatments using dynamic imaging approaches in contrast to the more common techniques described in Section 1.2. Section 2.2 explains the simplified physiological model and the governing system of partial differential equations (PDEs). In Section 2.3, the model is related back to the physical problem of measuring angiogenesis, the construct of the inverse problem is introduced, and the governing system of equations is spatially reduced to a system of ordinary differential equations (ODEs). The bounds of integration resulting from the reduction of PDEs into ODEs introduces a new term that is not easily measured. The need for this term is eliminated by the implementation of a simplification that is generally accepted in the radiology literature, as explained in Section 2.4. Section 2.5 provides an overview of several important results using the equations developed using the simplified system of ODEs. Section

2.6 discusses the creation of a baseline for numerical experimentation; this baseline is designed to mimic real patient data. A chapter summary is provided in Section 2.7.

## 2.1 Overview of Proposed Approach

As described in Section 1.2, the current approach to measuring the efficacy of a cancer treatment for an individual patient can take months, and during this time the patient may be suffering from side effects from an expensive and potentially ineffective treatment plan. The current non-invasive methods for measuring the efficacy of a particular drug for a patient is to use static contrast-enhanced images to determine the size of the tumor, then to try the drug for up to six months, and then to take another round of images to see if the tumor has grown. Using dynamic imaging techniques should decrease the trial period for each patient by measuring the blood supply directly, instead of waiting and watching for tumor growth. In this way the tumor could be treated effectively with less risk of over-treatment, under-treatment, or time wasted on a treatment that fails to work. With minimal modifications to the data collection process, this research proposes to use all the time-data from the sequence of images to identify parameters that indicate how blood is flowing in the region of the tumor, such as perfusion, permeability-surface-area product, and relative volumes of the plasma and extracellular-extravascular space [4, 7]. Therefore, if a treatment only takes a few days to start impacting blood flow to the tumor, the efficacy of this treatment can be measured within weeks [8].

## 2.2 Single Capillary Model

In an effort to make this work accessible to the radiology community, the model used is generally accepted as the building block for research in this field [4].

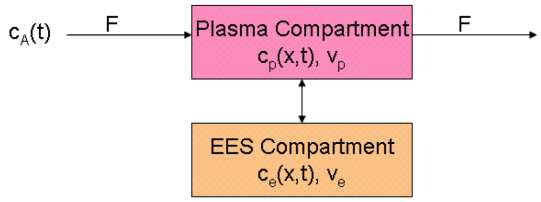


Figure 2.1: This quasi-1D model has two compartments through which contrast agent flows in time and space: the plasma compartment inside the capillary; the extracellular-extravascular space (EES) immediately surrounding the capillary. $c_A(t)$ represents the flow into the capillary from the artiole, $F$ represents the flow perfusion, $c_p(x,t)$ and $c_e(x,t)$ represent the concentration of tracer in the plasma and EES compartments respectively, and $v_p$ and $v_e$ represent the respective volumes of the two compartments.

The simple two compartment model illustrated in Figure 2.1 represents the flow of contrast agent into, through, and out of an average capillary. Naturally, the region of interest in a human body will have a very large number of capillaries feeding both the tumor and the surrounding healthy tissue, however, modeling the complexities of the actual human body would be computationally difficult and expensive and is probably unnecessary. Trends can be identified by studying the changes between pre-treatment and post-treatment parameters for an average of all the capillaries. Thus, in this model, the single capillary can be thought of as either an average capillary or as a representative conglomerate of all the capillaries in the region of interest.

The first compartment, called the plasma compartment, represents the region inside the capillary. The relative volume of this compartment is presumed to be a constant value, $v_p$. The tracer enters the capillary through the artiole at a flow perfusion rate, $F$. The concentration of the contrast agent entering the capillary, denoted $c_A(t)$, is a measurable quantity, since the tracer is injected upstream of the capillary and blood vessels are largely impermeable except the capillaries. The tagged blood flows into the capillary, and due to the concentration gradient, oncotic or *colloid osmotic* pressure pushes the tracer out of the capillary into the second compartment in the model, the extravascular extracellular space or EES compartment; this com-

partment is also referred to as the interstitial space. As with the first compartment, the relative volume of the EES compartment, $v_e$, is presumed to remain constant for the duration of the CT or MRI scan. In Figure 2.1, note the arrow between the two compartments is bidirectional; when there is more tracer in the EES compartment than in the capillary, the oncotic pressure will be reversed and the capillary will re-absorb some of the tracer. In other words, the flow across the capillary wall is bidirectional. The rate at which tracer can travel across this membrane is dependent on both the surface area of the capillary wall and the permeability of this wall. As these two characteristics act in tandem to either promote or limit blood flow across the capillary wall, they are combined into a single quantity, the permeability surface area product, denoted $P$. Since neither factor should change significantly in the time scale of an imaging session, it is presumed that this product, $P$, is a constant.

This physical system is mathematically represented using basic mass transport conservation equations, resulting in a linear system of two partial differential equations (PDEs):

$$v_p \frac{\partial c_p(x,t)}{\partial t} = -FL\frac{\partial c_p(x,t)}{\partial x} - P(c_p(x,t) - c_e(x,t)), \tag{2.1}$$

$$v_e \frac{\partial c_e(x,t)}{\partial t} = P(c_p(x,t) - c_e(x,t)), \tag{2.2}$$

subject to: initial conditions $c_p(x, t = 0) = 0$ and $c_e(x, t = 0) = 0$, and boundary condition $c_p(x = 0, t) = c_A(t)$, where $c_p(x,t)$ is the concentration of contrast agent in the plasma, $c_e(x,t)$ is the concentration of contrast agent in the EES, $F$ is the blood flow perfusion, $L$ is the length of the capillary, $P$ is the permeability surface area product, $v_p$ is the volume fraction of plasma compartment in the region of interest, and $v_e$ is the volume fraction of EES compartment in the region of interest. Without loss of generality, the problem can be scaled to the length of the capillary, $L = 1$,

thus (2.1) can be rewritten:

$$v_p \frac{\partial c_p(x,t)}{\partial t} = -F \frac{\partial c_p(x,t)}{\partial x} - P(c_p(x,t) - c_e(x,t)). \tag{2.3}$$

Alternatively, (2.2) and (2.3), may be written as a system of linear scalar PDEs with a source term as:

$$\begin{pmatrix} v_p & 0 \\ 0 & v_e \end{pmatrix} \begin{pmatrix} c_p \\ c_e \end{pmatrix}_t = - \begin{pmatrix} F & 0 \\ 0 & 0 \end{pmatrix} \begin{pmatrix} c_p \\ c_e \end{pmatrix}_x - P \begin{pmatrix} 1 & -1 \\ -1 & 1 \end{pmatrix} \begin{pmatrix} c_p \\ c_e \end{pmatrix}. \tag{2.4}$$

For the time period of the imaging, it is assumed that the coefficients $F$, $P$, $v_p$, and $v_e$ are constant. Using Ficks First Law, the rate of change of tracer in the plasma compartment is dependent on the amount of tracer flowing through the capillary, into the capillary from the artiole and out of the capillary into the venule, and the amount transferred out the capillary through the porous membrane into the EES. Notice that the only source of concentration change in the EES is exactly equal and opposite to last term in the plasma compartment equation. This term represents passive transport across the capillary membrane into the interstitial space. This makes sense because the only doorway for the tracer into/out of the EES is across the membrane of the capillary. This term is the diffusion term, so the direction of flow is dictated by the concentrations of the two compartments; when the concentration is higher is the plasma, tracer will flow out of the capillary, and vice versa. Remember that $P$ represents the permeability surface area product; this value defines how easily the tracer can pass through the endothelial membrane of the capillary; the higher $P$ is, the more efficient the capillary is at releasing and accepting particles such as oxygen or tracer.

The art of mathematical modeling is balancing reduced complexities with reasonable justifications and an understanding the potential source of error associated with each simplification and assumption. For this reason, it is important to explore

the assumptions associated with this model and validity of those assumptions. The model is a very simplified model of the actual complexities of the human body. The most obvious simplifications of this model are the use of a single capillary to represent a complex network of many capillaries, the lack of a lymphatic system, the assumption that the tracer is equally soluble in both the EES and the plasma, and the assumption that the permeability across the capillary membrane is the same in both directions.

This model only looks at a single capillary, yet the results are used to perform analysis on very complicated human tissue filled with numerous microvessels (arterioles, capillaries, venules, and shunts) that represent dynamic pathways that can change to help the body maintain its core temperature and meet regional oxygen demands. At first glance, it seems this assumption is stating that all capillaries in the region of interest are identical. That assumption would not be very accurate. A human capillary averages 8 microns in diameter and can range from 4 to 20 microns in diameter, and the typical length ranges between 750 microns to 1 mm [9]. However, this simplification is simply stating that the main interest lies in understanding the global behavior in a particular patient which can be measured on a larger scale. Thus, with such a large number of capillaries, reducing the global behavior to an average model of a single capillary is still a useful method for measuring blood flow parameters.

This model does not have a compartment to represent the lymphatic system, which could also remove tracer from the EES. Fortunately, this simplification should not cause significant errors, as the images of interest are taken over a relatively short time period. Additionally, it should be noted that several types of contrast agent are not collected by the lymphatic system.

It is assumed that the tracer is an equally soluble solute in the EES and in the plasma. This is a reasonable assumption, as both solvents are primarily water with many physiological similarities.

The last major assumption of this model is that the permeability is the same in both directions. For this to be true, there can only be passive transport, and the viscosity and hydrostatic pressure must be the same on both sides of the membrane. Both of these requirements may not be true, and it should not be too difficult to modify the model to reflect a non-isodirectional transport, i.e. have different values of $P$ for contrast agent entering the EES and for contrast agent leaving the EES. However, for the initial investigations, following in the footsteps of others, it is assumed that the permeability is the same both directions. The underlying principles to justify this simplification are that the tracers used should not induce an active transport phenomenon, thus satisfying the first requirement for only passive transport. The second requirement of matching viscosities and hydrostatic pressures is more difficult. The viscosity of blood and interstitial fluid are complex enough topics to cover an entire thesis, but suffice it to say that it is assumed that they are locally similar. The pressure in the capillaries is typically between 15-30 mmHg higher than that of the interstitial space [1], however, it is unclear how dramatically this will impact the results. Again, remember that this assumption can be eliminated fairly easily, and this topic is left for future exploration.

## 2.3 Reducing the Equations and Introducing the Inverse Problem

Due to the simplicity of the model relative to the geometric complexity of the body, there is no strong correlation between any spatial data in the test images and the spatial relationships in the model. To bridge the gap between the model and the data available from the medical imaging, the spatial relations are removed by averaging over the length of the capillary in the model. For the image data, each pixel intensity is summed over the whole image for each time step to give the signal intensity. For the equations, both PDEs (2.2) and (2.3), are spatially integrated along the length

of the capillary, resulting in a system of ordinary differential equations (ODEs). In the equations below, the bars indicate spatial averages.

$$v_p \frac{\mathrm{d}\bar{c_p}(t)}{\mathrm{d}t} = F(c_A(t) - c_V(t)) - P(\bar{c_p}(t) - \bar{c_e}(t)), \tag{2.5}$$

$$v_e \frac{\mathrm{d}\bar{c_e}(t)}{\mathrm{d}t} = P(\bar{c_p}(t) - \bar{c_e}(t)), \tag{2.6}$$

subject to: initial conditions $\bar{c_e}(0) = 0$ and $\bar{c_p}(0) = 0$, and where $c_A(t) = c_p(x = 0, t)$ is the flow into the model capillary from the artiole and $c_V(t) = c_p(x = L, t)$ is the flow from the capillary out of the model into the venule. Alternatively, these equations can be written in the form of a system of ODEs with a source term as:

$$\begin{pmatrix} v_p & 0 \\ 0 & v_e \end{pmatrix} \frac{d}{dt} \begin{pmatrix} \bar{c_p} \\ \bar{c_e} \end{pmatrix} = -P \begin{pmatrix} 1 & -1 \\ -1 & 1 \end{pmatrix} \begin{pmatrix} \bar{c_p} \\ \bar{c_e} \end{pmatrix} + F \begin{pmatrix} c_A(t) - c_V(t) \\ 0 \end{pmatrix}. \tag{2.7}$$

These equations can be related back to the signal intensity of the sequence of images through following relationship, as the signal intensity of the entire image is given by the sum of the contrast agent in each of the two compartments:

$$S(t) = v_p \bar{c_p}(t) + v_e \bar{c_e}(t). \tag{2.8}$$

The medical imaging problem in question is an inverse problem, i.e. in addition to knowing the initial conditions and the boundary condition, some information about the solution is known, however the coefficients are unknown. In this application, the contrast agent entering the capillary via the arteriole can be measured at each time step. Additionally, the signal intensity of each pixel in a single image in the sequence can be summed to calculate the total signal intensity at each time step. Using this information, the problem is to determine the parameters that characterize the blood flow in the region: perfusion, the permeability surface area product of the capillaries, and the volumes of the capillaries and the surrounding tissue. Correlating this back

to the system of ODEs (2.7), given $c_A(t)$ and signal intensity $S(t)$, the goal is to determine the constant coefficients $F$, $P$, $v_p$, and $v_e$ for each set of test data from a particular patient.

## 2.4 Morales and Smith Simplification

The inflow term, $c_A(t)$, is measurable; it is the amount of tracer injected into the capillary as a function of time. Also, the sum of the solution to the ODEs, weighted by the relative volume of each compartment, is also discretely known in time, as this can be determined from the sum of the signal intensity of the pixels in the images in the region of interest. However, the outflow term, $c_V(t)$, is not known, and it cannot be explicitly measured easily. Much of the work that has been done on this problem makes an assumption on the outflow term to simplify the problem; specifically using the mathematical representation of capillary re-uptake as proposed by Morales and Smith in 1948 [14] and applied to this problem by Brix et al. in 1999 [4]:

$$c_A(t) - c_V(t) = \frac{1}{r}\Big(c_A(t) - \bar{c_p}(t)\Big), 0 \leq r \leq 1, \tag{2.9}$$

where $r$ is a tunable parameter. By substituting this assumption into the ODEs, one obtains the following modified system of equations:

$$v_p \frac{\mathrm{d}\bar{c_p}(t)}{\mathrm{d}t} = f(c_A(t) - \bar{c_p}(t)) - P(\bar{c_p}(t) - \bar{c_e}(t)), \tag{2.10}$$

$$v_e \frac{\mathrm{d}\bar{c_e}(t)}{\mathrm{d}t} = P(\bar{c_p}(t) - \bar{c_e}(t)), \tag{2.11}$$

where $f = \frac{F}{r}$ is the apparent flow rate. Alternatively, (2.10) and (2.11) can be written as:

$$\begin{pmatrix} v_p & 0 \\ 0 & v_e \end{pmatrix} \frac{d}{dt} \begin{pmatrix} \bar{c}_p \\ \bar{c}_e \end{pmatrix} = \begin{pmatrix} -(f+P) & P \\ P & -P \end{pmatrix} \begin{pmatrix} \bar{c}_p \\ \bar{c}_e \end{pmatrix} + \begin{pmatrix} f c_A(t) \\ 0 \end{pmatrix}. \tag{2.12}$$

This modified system has been the starting point for a number of studies in this field. In addition to using this simplified model to analyze real patient data [10, 11], radiologists and mathematicians have proposed various methods to improve parameter measurements starting with this modified system of equations, ranging from enhancing the model with more compartments [12] to more mathematically stable methods [13] to solve the inverse problem of determining the coefficients; some of these results are explained in Section 2.5.

## 2.5 Several Results Using the Morales and Smith Simplification

Using the simplified system (2.12), Gottlieb and Don developed several important results [13]. First, given parameters $f$, $v_p$, $P$, and $v_e$, the inflow term $c_A(t)$, and initial conditions $\bar{c}_p(0) = \bar{c}_e(0) = 0$, they show that (2.12) can be solved analytically by:

$$\bar{c}_p(t) = \frac{f}{v_p v_e(\lambda_1 - \lambda_2)}\big((P + v_e\lambda_1)I_1 - (P + v_e\lambda_2)I_2\big), \tag{2.13}$$

$$\bar{c}_p(t) = \frac{f}{v_p v_e(\lambda_1 - \lambda_2)}(PI_1 - PI_2), \tag{2.14}$$

where $I_1$ and $I_2$ are given by:

$$I_1 = \int_0^t e^{\lambda_1(t-\tau)} c_A(\tau)d\tau, \tag{2.15}$$

$$I_2 = \int_0^t e^{\lambda_2(t-\tau)} c_A(\tau)d\tau, \tag{2.16}$$

and $\lambda_1$ and $\lambda_2$ are the solutions to the characteristic equation:

$$v_e v_p\lambda^2 + \lambda\big(fv_e + P(v_p + v_e)\big) + fP = 0. \tag{2.17}$$

The next important result is that the inverse problem as defined in Section 2.3 can be solved explicitly. Given $c_A(t)$ and $S(t)$, the apparent flow, $f$, is:

$$f = \begin{cases} \frac{S'(0)}{c_A(0)} & \text{if } c_A(0) \neq 0 \\ \frac{S''(0)}{c'_A(0)} & \text{if } c_A(0) = 0. \end{cases} \tag{2.18}$$

The concentration of the contrast agent in the plasma compartment, $\bar{c}_p$, is then recovered using:

$$\bar{c}_p(t) = c_A(t) - \frac{1}{f} S'(t). \tag{2.19}$$

Knowing $\bar{c}_p(t)$, the volume of the plasma compartment, $v_p$, is found by:

$$v_p = \begin{cases} \frac{S'(0)}{\bar{c}'_p(0)} & \text{if } c_A(0) \neq 0 \\ \frac{S''(0)}{\bar{c}''_p(0)} & \text{if } c_A(0) = 0. \end{cases} \tag{2.20}$$

The permeability surface area product, $P$, is given as:

$$P = \begin{cases} -f + f\frac{c'_A(0)}{\bar{c}'_p(0)} - v_p\frac{\bar{c}''_p(0)}{\bar{c}'_p(0)} & \text{if } c_A(0) \neq 0 \\ -f + f\frac{c''_A(0)}{\bar{c}''_p(0)} - v_p\frac{\bar{c}'''_p(0)}{\bar{c}''_p(0)} & \text{if } c_A(0) = 0. \end{cases} \tag{2.21}$$

The concentration of the contrast agent in the EES compartment, $c_e(t)$, can be found using:

$$\bar{c}_e(t) = \frac{v_p}{P}\bar{c}'_p(t) + \frac{f+P}{P}\bar{c}_p(t) - \frac{f}{P}c_A(t). \tag{2.22}$$

Using all of the results above, the last coefficient, $v_e$, is recovered by:

$$v_e = \begin{cases} \frac{P\bar{c}'_p(0)}{\bar{c}'''_e(0)} & \text{if } c_A(0) \neq 0 \\ \frac{P\bar{c}''_p(0)}{\bar{c}^{(4)}_e(0)} & \text{if } c_A(0) = 0. \end{cases} \tag{2.23}$$

It is important to note that if given the separate concentration trajectories, $\bar{c}_p(t)$

and $\bar{c}_e(t)$, in lieu of the combined value $S(t)$, the solution will not be unique. Specifically, if the set $\{f, v_p, P, v_e\}$ is a solution to the inverse problem given $c_A(t)$, $\bar{c}_p(t)$, and $\bar{c}_e(t)$, then the set $\{zf, zv_p, zP, zv_e\}$ is also a solution for any number $z$.

Due to the high number of derivatives required to use the explicit solution (see (2.23)), this method is unstable, and some results are not physically possible, such as negative values for $v_e$. To remedy this, an alternative approach is also suggested. Substituting parts of the direct solution to the inverse problem into the modified system of ODEs (2.12), the following equation is obtained:

$$\frac{Pf}{v_e v_p} S(t) + \left( \frac{f}{v_p} + P \frac{v_e + v_p}{v_e v_p} \right) S'(t) + S''(t) - Pf \frac{v_e + v_p}{v_e v_p} c_A(t) - f c_A'(t) = 0. \quad (2.24)$$

Recall for the inverse problem, $S(t)$ and $c_A(t)$ are known, at least in a discrete sense for each image in time, and their derivatives can be computed. The four coefficients of the ODE system, $f$, $v_p$, $P$, and $v_e$, are derived through an $L_2$ optimization of (2.24). Although this method is more stable than the explicit solution to the inverse problem, it still produced negative results for the volume of the EES compartment, $v_e$.

The above results obtained by Gottlieb and Don [13] raise concerns about the model using the modified ODE system (2.12) as the physics are not accurately recovered even using multiple mathematical approaches.

## 2.6 Baseline Problem

While the goal of this research is to develop methods for determining the blood flow parameters for actual cancer patients, it is not useful to test new methods on actual patient data. Patient data only contains the boundary condition, $c_A(t)$, and the signal intensity, $S(t)$, and the coefficients are not known. Therefore, when calculating the coefficients of real patient data, there is no physical result available for validation and verification of the computational methods. Thus, for the purposes

of testing the ideas presented in this thesis, computational baseline data is used in lieu of actual patient data. Using known coefficients, known initial conditions, and known boundary conditions, the simplified ODEs (2.12) can be solved numerically to obtain the average concentration of contrast agent in each compartment at each time-step, $\bar{c_p}(t)$ and $\bar{c_e}(t)$. The resulting signal intensity can then be calculated using (2.8).

To emulate the parabolic shape that naturally occurs in actual patient data as shown in Figure 2.2, the boundary condition, (2.25), was selected (see Figure 2.3) [13]; the baseline time is scaled such that the contrast agent is injected over a time period of 1.

$$c_A(t) = -(t - 0.5)^2 + 0.25. \tag{2.25}$$

Next, coefficients values were chosen to match the calculated signal intensity with the general shape of the signal intensity graph obtained from actual patient data.

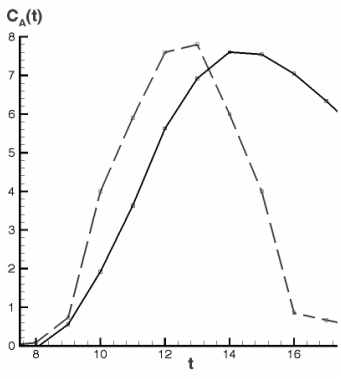


Figure 2.2: Actual patient data. Dashed line: injected $c_A(t)$. Solid line: $S(t)$.

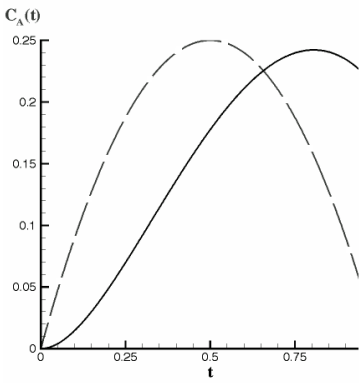


Figure 2.3: Baseline data. Dashed line: injected $c_A(t)$. Solid line: $S(t)$.

This equation for the boundary condition, (2.25), is used as a baseline case for developing datasets for the numerical experiments described in Chapter 3 and Chapter 4. In Chapter 3, this baseline problem is used to parametrically explore the impact of each coefficient on the signal intensity. In Chapter 4, results from numerical

experimentation will be presented for two sets of data derived from this baseline problem.

## 2.7 Summary

This chapter explained several important results from the existing literature. After presenting an argument for the need for dynamic imaging methods to measure angiogenesis in tumor regions, a two-compartment model was introduced along with the governing system of PDEs. As the spatial relationships between the model and the physical data are not correlated, the PDEs were then integrated spatially to obtain a system of ODEs. The inverse problem was presented: a weighted sum of the solutions to the ODEs is known, but the constant coefficients are unknown. One of the terms in the ODEs, specifically the term representing the outflow of contrast agent through the venules, is difficult to measure; a simplification for capillary reuptake was applied to remove the need for this term in the equations, resulting in a modified system of ODEs. Several results were presented using this modified system of ODEs: a direct solution to the ODEs; an explicit solution to the inverse problem; an alternative least squares optimization technique to solve the inverse problem. For the purposes of testing new methods, an analytical set of baseline data was required; thus one was created to emulate patient data.

# Chapter 3

# Parametric Study of the Relationships between Signal Intensity and the Four Coefficients

The trajectory of the signal intensity, $S(t)$, is a function of the four coefficients, $F$, $v_p$, $P$, and $v_e$. In order to better understand the dependence between $S(t)$ and each of the coefficients, in this chapter, the relationships are explored through parametric evaluation. As each coefficient is varied, the mathematical results are explained by relating the phenomenology back to the physical system the model represents. Section 3.1 briefly explains the basic shape of the trajectory of $S(t)$. Section 3.2 focuses on the relationships between the trajectory of $S(t)$ and the four coefficients that arise from the modified system of ODEs (2.12). After a discussion of the numerical techniques used to evaluate $S(t)$, each coefficient is examined separately in Sections 3.2.1 through 3.2.4. Section 3.3 looks at how the signal intensity, $S(t)$, will vary with the four coefficients based on the relationships defined by the system of PDEs (2.4). The four parameters are each examined separately in Sections 3.3.1 through 3.3.4. In Section 3.4, the results arising from the system of ODEs (2.12) are compared with and contrasted against the results arising from the system of PDEs (2.4). Section

3.5 provides a summary of this chapter.

## 3.1 Basic Shape of $S(t)$ Trajectory

Figure 3.1 shows a sample trajectory of the signal intensity on the same set of axes as the concentration of the tracer entering the system, $c_A(t)$ (see Section 2.6). As tracer begins to enter the capillary, the total signal intensity slowly begins to rise. It does not follow the exact trajectory of the concentration curve, $c_A(t)$; the signal intensity is weighted by the relative volumes of the compartments. Then, as the tracer moves along the capillary, some is transported across the membrane into the EES compartment. While tracer in both compartments is included in the total signal intensity, the volume of a compartment plays a role in the significance of that term's contribution. The ease of transport between these two compartments is regulated by the permeability surface area product, $P$. At some time, $t^*$, the initial amounts of contrast agent will have traveled the length of the capillary and will begin to exit the system via the venule causing the total signal intensity to begin to fall; this time, $t^*$, is dependent on the flow perfustion rate, $F$.

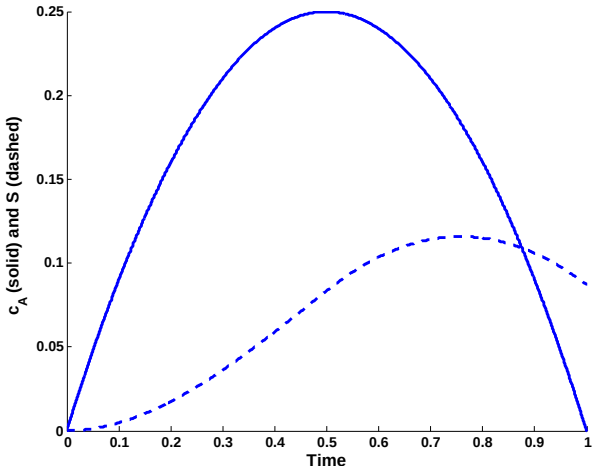


Figure 3.1: Sample Plot of $S(t)$.

## 3.2 Varying the Coefficients in the ODEs

A set of numerical experiments was developed to measure the effect of each coefficient in the ODEs (2.12) on the signal intensity, $S(t)$. In these experiments, it is assumed that $c_A(t)$ is given as (2.25), that the initial conditions are known to be $\bar{c_p}(0) = 0$ and $\bar{c_e}(0) = 0$, and that the values of the four coefficients are given. Then, using the forward Euler finite difference scheme shown in (3.1) and (3.2), the average concentration of the contrast agent in the plasma compartment, $\bar{c_p}^k$, and average concentration of the contrast agent in the EES compartment, $\bar{c_e}^k$, are computed for each time-step, $k$. Here $k$ represents the current timestep; the time is computed by $t = k\Delta t$. For the calculations throughout this section, $\Delta t = 0.0002$, and recalling that the problem has been scaled in time, $T = 1$ (see Section 2.6), thus $k = 0 : 5000$.

$$\bar{c_p}^{k+1} = \bar{c_p}^k + \frac{\Delta t}{v_p}\Big( -(f+P)\bar{c_p}^k + P\bar{c_e}^k + Fc_A^k \Big), \tag{3.1}$$

$$\bar{c_e}^{k+1} = \bar{c_e}^k + \frac{P\Delta t}{v_e}\Big( \bar{c_p}^k - \bar{c_e}^k \Big), \tag{3.2}$$

given $c_A^k$ for $k \geq 0$ and initial conditions $\bar{c_p}^0 = \bar{c_e}^0 = 0$.

Other numerical methods were tested, however, for this problem, the forward Euler scheme was sufficiently accurate and very efficient.

Then the signal intensity at the $k^{th}$ time-step, $S^k$, is computed by adding the concentrations in each compartment weighted by the compartment volume. This relationship follows directly from the definition of the signal intensity function from (2.8):

$$S^k = v_p\bar{c_p}^k + v_e\bar{c_e}^k. \tag{3.3}$$

In each of the following four sections, one coefficient will be varied while the others are kept constant. The baseline coefficients are $f = 1$, $v_p$=0.5, $P = 0.05$, and

$v_e = 0.7$ except where stated otherwise.

### 3.2.1 Varying $f$

Recall the coefficient, $f$, represents the apparent flow rate. Therefore, an increase in $f$ will cause an increase in the rate at which the contrast agent enters the system, an increase in the total amount of contrast agent in the system, and an earlier departure of contrast agent via the venule. In terms of the graph of signal intensity in time, $S(t)$, an increase in perfusion causes the curve to rise sooner, the maximum value of $S(t)$ will increase, and the decreasing section of the graph will have a steeper slope. Figure 3.2 illustrates this behavior for $f = \{0.5, 1, 1.5, 2\}$.

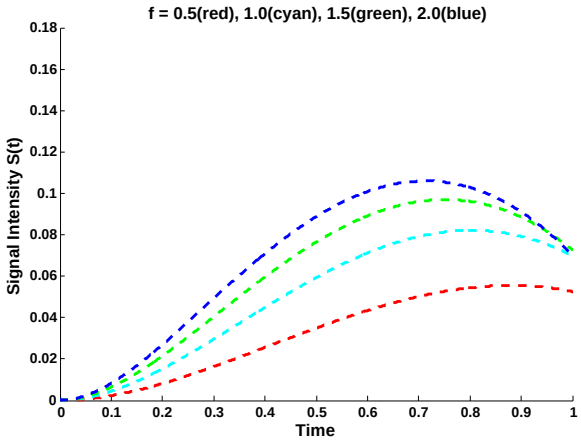


Figure 3.2: Changes in $S(t)$ due to varying $f$.

### 3.2.2 Varying $v_p$

The coefficient, $v_p$ represents the volume of the plasma compartment, or more fundamentally, the volume contained within the capillary. Increasing $v_p$ causes an increase in the amplitude; it also causes the initial onset of the rise of the signal intensity curve to come slightly earlier and the signal is elongated in time. The increase in

amplitude makes physical sense because if the same concentration of tracer exists in a larger volume, then there should be more tracer overall, which explains the increase in signal intensity. Also, since the apparent flow rate, $f$, is a volumetric flow rate, if the volume is increased and the length stays the same, the actual velocity is slower which increases the time until the signal intensity peaks. For the same reason the decrease in signal intensity also takes more time for higher values of $v_p$. Figure 3.3 illustrates this behavior for $v_p = \{0.3, 0.5, 0.7, 0.9\}$.

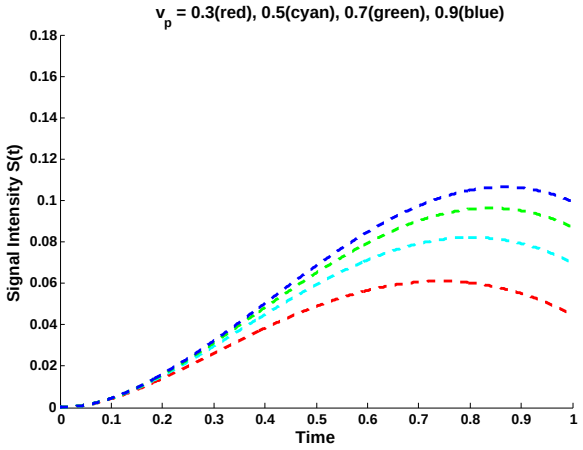


Figure 3.3: Changes in $S(t)$ due to varying $v_p$.

### 3.2.3 Varying $P$

The coefficient $P$ represents the permeability-surface area product. Increasing $P$ increases the maximum amplitude by prolonging the growth of the signal, in other words, the peak and fall of the curve are shifted to the right. This makes sense because if the permeability-surface area product is higher, more of the tracer will be able to exit the capillary into the EES versus flowing out of the region of interest via the venule. In this way, the tracer continues to contribute to the signal intensity for a longer period of time as it is still contained within the overall region of interest. Figure 3.4 illustrates this behavior for $P = \{0.05, 1.0, 5.0, 10\}$. It should be noted

that a healthy capillary will have a very low permeability, on the lower end of this scale of $P$ values, while an unhealthy capillary can have $P$ values of over 20.

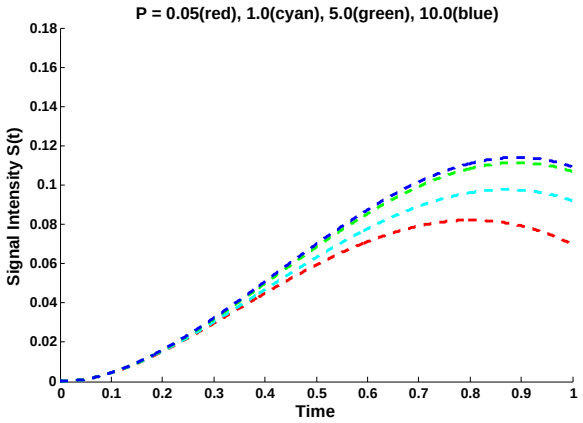


Figure 3.4: Changes in $S(t)$ due to varying $P$.

### 3.2.4 Varying $v_e$

Figure 3.5 shows how changes in the volume of the EES compartment impact the signal intensity for $v_e = \{0.1, 0.3, 0.5, 0.7\}$. The reason only one curve is visible in the figure is because all the lines are identical. When the permeability surface area product is very low, in this case $P = 0.05$, not much contrast agent has an opportunity to cross the capillary membrane into the EES compartment. Thus for low $P$ values, the value of $v_e$ has negligible impact on the behavior of the signal intensity curve, $S(t)$.

Figure 3.6 shows the results of a similar numerical experiment, only in this case, the permeability surface area product was increased to $P = 10$. Due to this increased value of $P$, contrast agent can easily pass through the capillary walls and enter the EES compartment, thus $v_e$ will play a role in the signal intensity curve. As the volume of the EES compartment is increased, the total signal intensity also increases. Additionally, it takes longer for the contrast agent to be extracted from the region

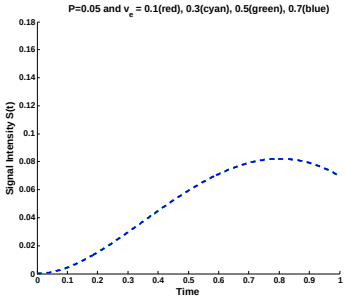


Figure 3.5: Changes in $S(t)$ due to varying $v_e$ when $P$ is small.

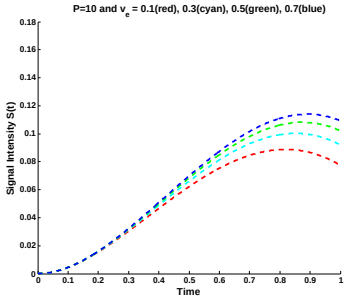


Figure 3.6: Changes in $S(t)$ due to varying $v_e$ when $P$ is large.

of interest.

Together, these two experiments illustrate the strong co-dependence of these two coefficients, $P$ and $v_e$.

## 3.3 Varying the Coefficients in the PDEs

Section 3.2 explored the relationships between each of the coefficients and the signal intensity curve using the simplified system of ODEs (2.12). In this section, these relationships will be explored through the use of the original system of PDEs (2.4). The results should be similar, and in Section 3.4, the two sets of results will be compared.

As in Section 3.2, a set of numerical experiments was developed to measure each coefficient's impact on the signal intensity, $S(t)$. In these experiments, it is assumed that boundary condition is given by $c_p(x = 0, t) = c_A(t)$ where $c_A(t)$ is given by (2.25), that the initial conditions are known to be $c_p(x, t = 0) = 0$ and $c_e(x, t = 0) = 0$, and that the values of the four coefficients are given.

Then, using the forward Euler finite difference scheme shown in (3.4) and (3.5), the concentration of the contrast agent in the plasma compartment, $c_{p_j}^{\ k}$, and concentration of the contrast agent in the EES compartment, $c_{e_j}^{\ k}$, are computed at each grid point, $j$, for each time-step, $k$. Here $k$ represents the current timestep; the time

is computed by $t = k\Delta t$. The index $j$ represents the spatial step; the $x$-position for a given step is $x = j\Delta x$. For the calculations throughout this section, $\Delta t = 0.0002$, and the problem has been scaled in time to $T = 1$ (see Section 2.6), thus $k = 0 : 5000$; $\Delta x = 0.002$, and the length of the capillary has also been scaled to $L = 1$, thus $j = 0 : 500$.

$$c_{p_j}^{k+1} = c_{p_j}^{k} + \frac{\Delta t}{v_p}\Big( - \frac{F}{\Delta x}(c_{p_j}^{k} - c_{p_{j-1}}^{k}) - P(c_{p_j}^{k} - c_{e_j}^{k})\Big) \tag{3.4}$$

$$c_{e_j}^{k+1} = c_{e_j}^{k} + \frac{P\Delta t}{v_e}\Big(c_{p_j}^{k} - c_{e_j}^{k}\Big) \tag{3.5}$$

given the boundary condition $c_{p\ 0}^{k} = c_A^{k}$ for $k \geq 1$ and initial conditions $c_{p_j}^{0} = c_{e_j}^{0} = 0$.

Although other numerical schemes were tested for use in this problem, the method described above was sufficiently accurate and highly efficient.

Recall from Section 3.2, based on the definition of the signal intensity, (3.3) computed the signal intensity at each time-step using the spatially averaged values for the contrast agent in each compartment, $\bar{c}_p$ and $\bar{c}_e$. To use this equation, the concentrations in each of the compartments, $c_p(x,t)$ and $c_e(x,t)$, must be integrated spatially. The integration will be equivalent to the average value, as the length has been scaled to $L = 1$. After using the trapezoidal rule to perform the integration of the contrast agent concentrations in the plasma compartment and the EES compartment, the signal intensity at each time-step, $S^k$, is computed using (3.3).

In each of the following four sections, one coefficient will be varied while the others are kept constant. The baseline coefficients are $F = 1$, $v_p$=0.5, $P = 0.05$, and $v_e = 0.7$ except where stated otherwise.

### 3.3.1 Varying $F$

The coefficient, $F$, represents the perfusion; it can be thought of as a flow rate. The coefficient in the ODE (2.10), $f$, is derived from this parameter, $F$; thus the

relationship between $F$ and $S(t)$ are, not surprisingly, similar to the results shown for varying $f$ in Section 3.2.1. An increase in $F$ will cause an increase in the rate at which the contrast agent enters the system and in the total amount of contrast agent in the system. In terms of the graph of signal intensity in time, $S(t)$, an increase in perfusion causes the curve to rise sooner, and the maximum value of $S(t)$ will also increase. Figure 3.7 illustrates this behavior for $F = \{0.5, 1, 1.5, 2\}$.

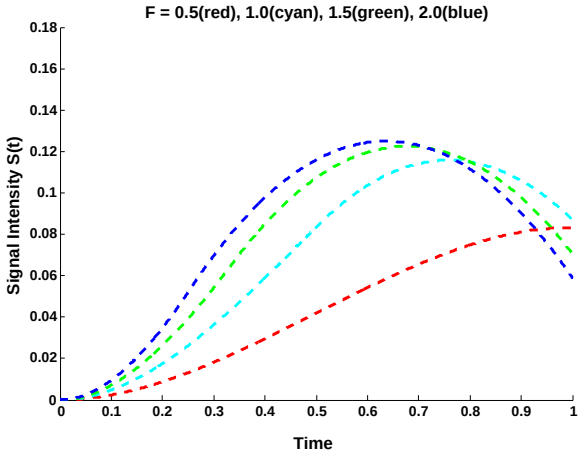


Figure 3.7: Changes in $S(t)$ due to varying $F$.

### 3.3.2 Varying $v_p$

The coefficient, $v_p$ represents the volume of the plasma compartment, or more fundamentally, the volume contained within the capillary. Similarly to the behavior demonstrated in Section 3.2.2, increasing $v_p$ causes an increase in the amplitude. It also causes the signal to be elongated in time. The increase in amplitude makes physical sense because if there is more volume of plasma with the same concentration of tracer in the volume, then there should be more tracer overall. Also, since $F$ is a volumetric flow rate, if the volume is increased and the length stays the same, the actual velocity is slower which increases the time until the signal intensity peaks. For the same reason the decrease in signal intensity also takes more time for higher

values of $v_p$. Figure 3.8 illustrates this behavior for $v_p = \{0.3, 0.5, 0.7, 0.9\}$.

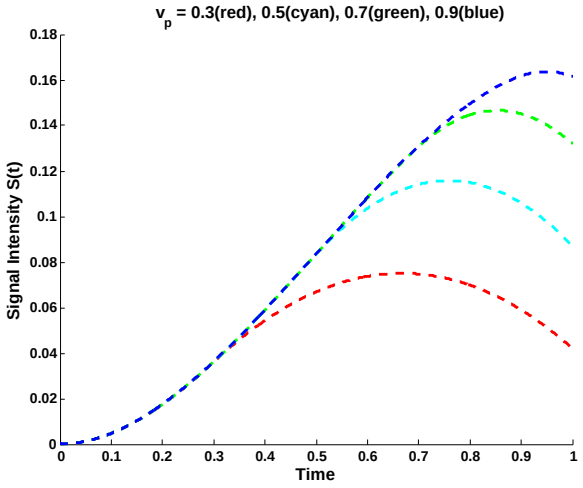


Figure 3.8: Changes in $S(t)$ due to varying $v_p$.

### 3.3.3 Varying $P$

The coefficient $P$ represents the permeability-surface area product. Changing $P$ does very little, if anything, to the initial rise of the signal intensity curve, $S(t)$. As shown in Section 3.2.3, increasing $P$ does increase the maximum amplitude by prolonging the growth of the wave, in other words, the peak and fall of the curve are shifted to the right. This makes sense because if the permeability-surface area product is higher, more of the tracer will be able to exit the capillary into the EES versus flowing out of the region of interest via the venule. In this way, the tracer continues to contribute to the signal intensity for a longer period of time as it is still contained within the overall region of interest. Figure 3.9 illustrates this behavior for $P = \{0.05, 1.0, 5.0, 10\}$.

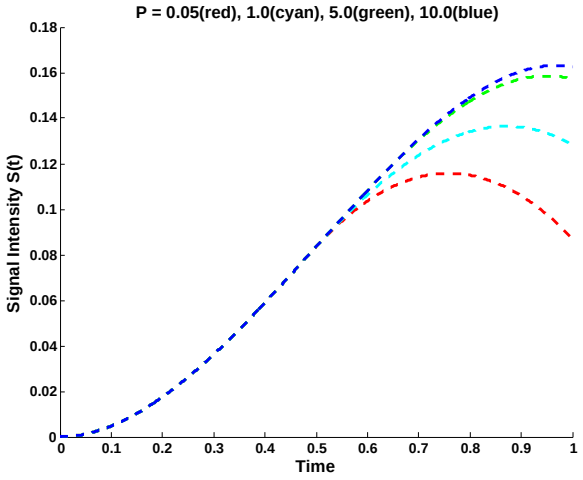


Figure 3.9: Changes in $S(t)$ due to varying $P$.

### 3.3.4 Varying $v_e$

The coefficient, $v_e$ represents the volume of the EES compartment. As explained in Section 3.2.4, when the permeability surface area product is very low, not much contrast agent has an opportunity to cross the capillary membrane into this compartment. Thus for low $P$ values, the value of $v_e$ has negligible impact on the behavior of the signal intensity curve, $S(t)$. This behavior is illustrated in Figure 3.10 for $P = 0.05$.

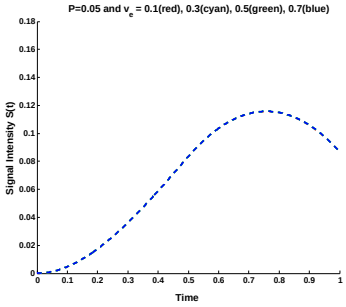


Figure 3.10: Changes in $S(t)$ due to varying $v_e$ when $P$ is small.

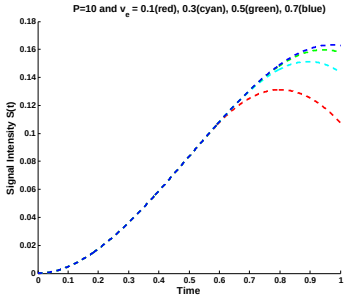


Figure 3.11: Changes in $S(t)$ due to varying $v_e$ when $P$ is large.

Figure 3.11 shows the results of a similar numerical experiment, only in this case,

the permeability surface area product was increased to $P = 10$. Due to this increased value of $P$, contrast agent can more easily enter the EES compartment, thus $v_e$ will play a role in the signal intensity curve. As the volume of the EES compartment is increased, the total signal intensity increases. Additionally, it takes longer for the contrast agent to be extracted from the region of interest.

## 3.4 Comparing the ODE and PDE Results

Section 3.2 and Section 3.3 used fairly similar methods to examine how the signal intensity depends on each of the four coefficients. Section 3.2 focuses on the signal intensity curve obtained using the system of ODEs (2.12), while Section 3.3 focuses on the signal intensity obtained from the system of PDEs (2.4). In this section, these two systems of equations are compared through the results of the parametric study above.

Figures 3.12 - 3.21 show side-by-side comparisons of the results presented in Sections 3.2 - 3.3. It is clear that while the general trends are similar, the results are not identical.

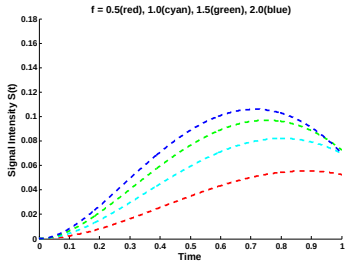


Figure 3.12: Changes in $S(t)$ due to Varying $f$ in ODEs.

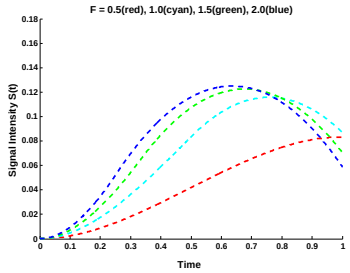


Figure 3.13: Changes in $S(t)$ due to Varying $F$ in PDEs.

Figures 3.22 - 3.25 each show an overlay of the PDE and ODE results on the same set of axes for one set of coefficient values. These coefficient values are given in Table 3.1. Notice, the coefficient $f$ is not defined to be equivalent to the coefficient $F$. The coefficient $f$ was defined in Section 2.4 as the apparent flow rate, given by

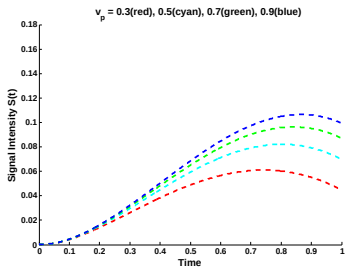


Figure 3.14: Changes in $S(t)$ due to Varying $v_p$ in ODEs.

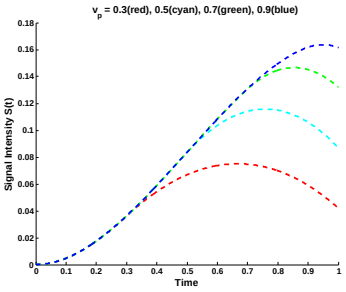


Figure 3.15: Changes in $S(t)$ due to Varying $v_p$ in PDEs.

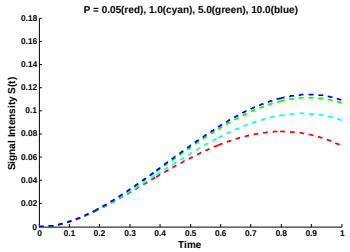


Figure 3.16: Changes in $S(t)$ due to Varying $P$ in ODEs.

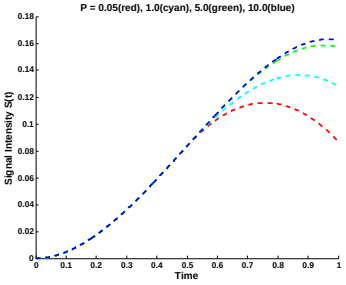


Figure 3.17: Changes in $S(t)$ due to Varying $P$ in PDEs.

$f = \frac{F}{r}$ where $r$ is a constant between zero and one. For the purposes of these initial comparisons, it is assumed that $r = 1$.

Table 3.1: Coefficient values for results shown in Figures 3.22 through 3.25.

| Figure Number | $F$ | $P$ | $v_e$ | $v_p$ |
|---|---|---|---|---|
| Figure 3.22 | 1.0 | 0.05 | 0.7 | 0.5 |
| Figure 3.23 | 2.0 | 1.0 | 0.5 | 0.3 |
| Figure 3.24 | 2.0 | 0.05 | 0.7 | 0.5 |
| Figure 3.25 | 1.0 | 1.0 | 0.7 | 0.5 |

In each case, the signal intensity computed from the PDE system (2.4) rises sooner and higher than that computed from the ODE system (2.12). One possible difference could come from the assumption that $r = 1$ in the relation $f = \frac{F}{r}$. However, no fixed value of $r$ seems to solve the discrepancy between the two curves. As an illustration, Figure 3.26 through Figure 3.29 compare the ODE and PDE results using one set

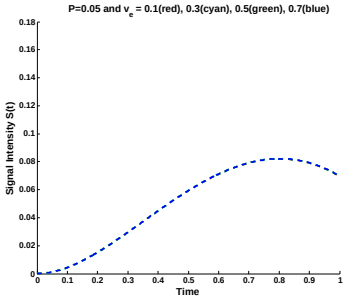


Figure 3.18: Changes in $S(t)$ due to Varying $v_e$ in ODEs, for small $P = 0.05$.

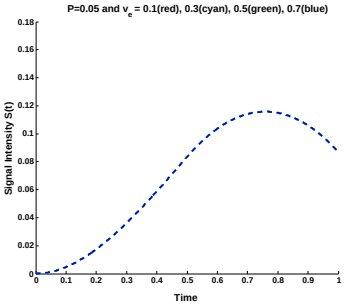


Figure 3.19: Changes in $S(t)$ due to Varying $v_e$ in PDEs, for small $P = 0.05$.

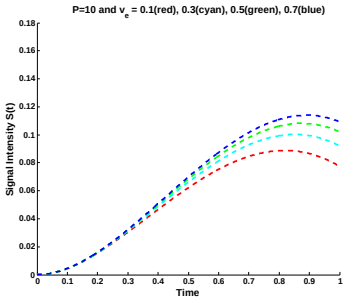


Figure 3.20: Changes in $S(t)$ due to Varying $v_e$ in ODEs, for large $P = 10$.

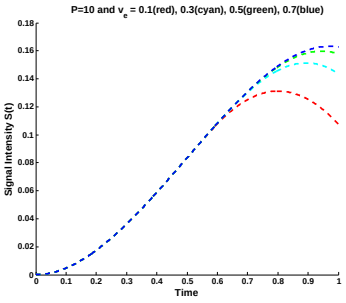


Figure 3.21: Changes in $S(t)$ due to Varying $v_e$ in PDEs, for large $P = 10$.

of coefficients $F = 1$, $P = 0.05$, $v_e = 0.7$, and $v_p = 0.5$, and different values of $r = \{1.0, 0.75, 0.5, 0.25\}$, thus $f = \{1, 1.\bar{3}, 2, 4\}$.

In Figure 3.26, the signal intensity calculated from the PDEs is higher than the signal intensity computed from the ODEs, and the maximum signal intensity is much higher in the PDE curve. In Figure 3.27, when $r$ is decreased to 0.75, the signal intensity from the ODEs is higher than the PDE solutions for early times, but around $t = 0.4$, the two curves cross, and again the PDE solution is higher. In Figure 3.28, when $r = 0.5$, the maximum values of $S(t)$ come close to matching for both curves, but note the entire ODE solution rises faster than the PDE solution. In Figure 3.29, when $r = 0.25$, the ODE solution is much higher than the PDE solution. Based on this sampling of results, it is clear that, at least for this case, there is not one fixed value of $r$ which will bring these two curves into close alignment with one

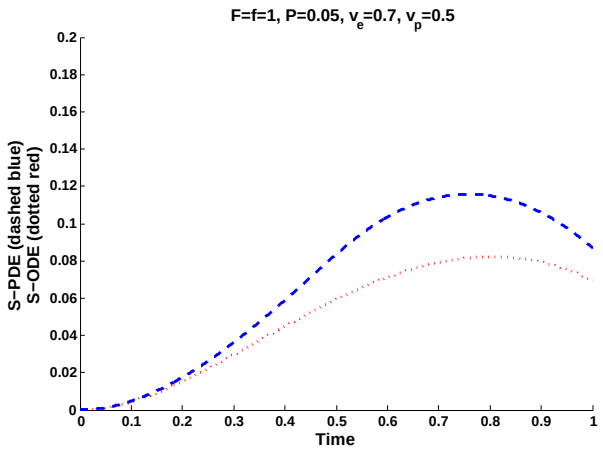


Figure 3.22: Comparison of ODE and PDE results for $F = f = 1$, $P = 0.05$, $v_e = 0.7$, and $v_p = 0.5$.

another.

This raises some questions about the origin of the simplified ODE system (2.12). The ODEs were derived through a two-step process. First, the original PDEs were spatially integrated, resulting in the system (2.7). Second, due to the difficulty in measuring the value $c_V(t)$ in (2.5), a simplification was introduced in Section 2.4. Implementing this simplification into (2.7) resulted in the system (2.12) which was used in the parametric study in Section 3.2.

Of these two steps in the derivation process, the simplification is the most likely source of concern. In Chapter 4, the validity of this simplification is further examined.

## 3.5 Summary

Through a parametric study, this chapter explored the effect of each of the four parameters on signal intensity. Section 3.2 presented the results of a set of numerical experiments on the ODEs (2.12) using a forward Euler scheme given by (3.1) and (3.2). Based on these experiments, it is shown that increasing perfusion, $F$, causes an earlier rise in signal intensity and an increase in the maximum value of signal

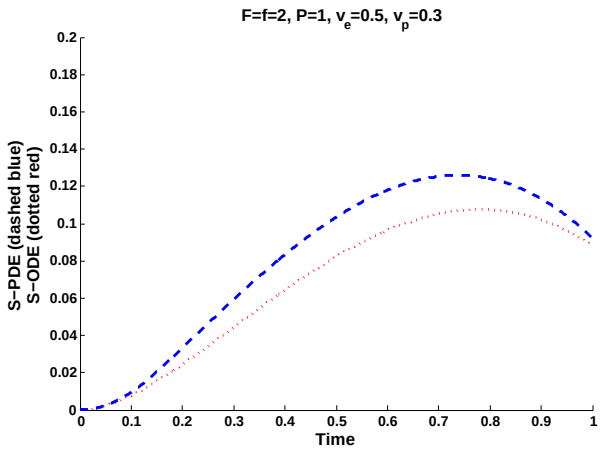


Figure 3.23: Comparison of ODE and PDE results for $F = f = 2$, $P = 1$, $v_e = 0.5$, and $v_p = 0.3$.

intensity over the range of $F$ values considered. Increases in the volume of the plasma compartment, $v_p$ , cause the signal intensity to ascend earlier and faster and to descend slower. Even large changes in the permeability surface area product, $P$, have minimal impact on the initial growth of the signal intensity, however, at later time, an increase in $P$ produces a higher maximum value of $S(t)$ and elongates both the ascent and descent of the signal in time. When coupled with a low value of $P$, the volume of the EES compartment, $v_e$, has effectively no impact on the signal intensity, however, in the presence of a higher permeability surface area product, an increase in $v_e$ produces a higher maximum value of $S(t)$ and an elongated signal in time. This set of results for varying $P$ and $v_e$ gives some indications about the coupling between these two parameters. Section 3.3 presented the results of a set of similar numerical experiments on the PDEs (2.4). Bewteen the ODE-based study and the PDE-based study, the trends were similar for each parameter, however, the results were not as close as expected. This led to an initial look at the tunable parameter, $r$, in the Morales and Smith simplification. For a single set of coefficient values, the PDE-based results were compared against the ODE-based results for four different values of $r$. None of these values reconciled the differences in the two solutions.

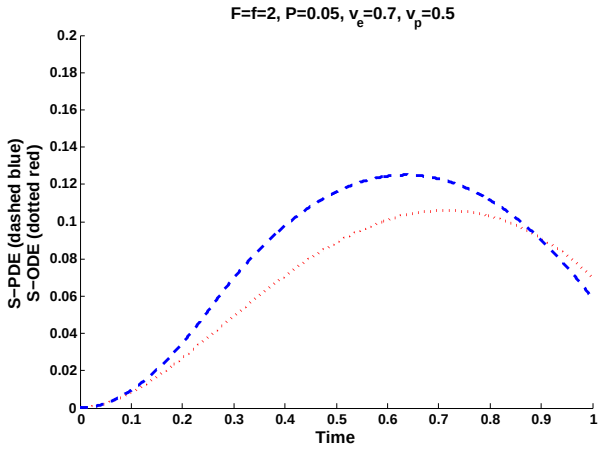


Figure 3.24: Comparison of ODE and PDE results for $F = f = 2$, $P = 0.05$, $v_e = 0.7$, and $v_p = 0.5$.

Chapter 4 will further examine the Morales and Smith simplification, particularly the assumption that $r$ is a constant.

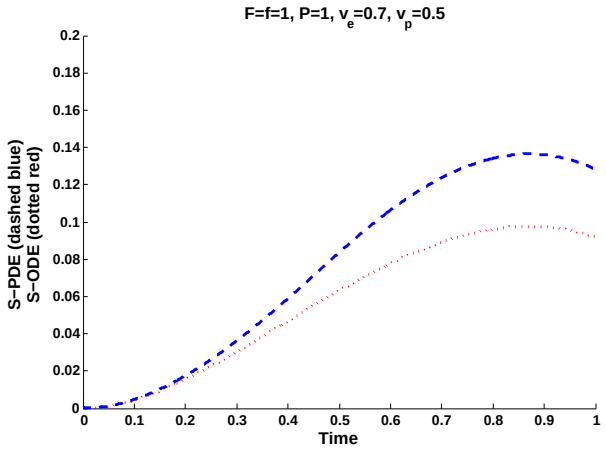


Figure 3.25: Comparison of ODE and PDE results for $F = f = 1$, $P = 1$, $v_e = 0.7$, and $v_p = 0.5$.

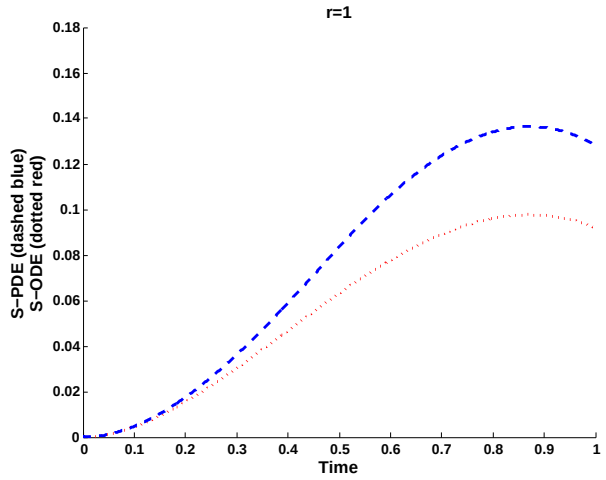


Figure 3.26: Comparison of ODE and PDE results for $r = 1.0$.

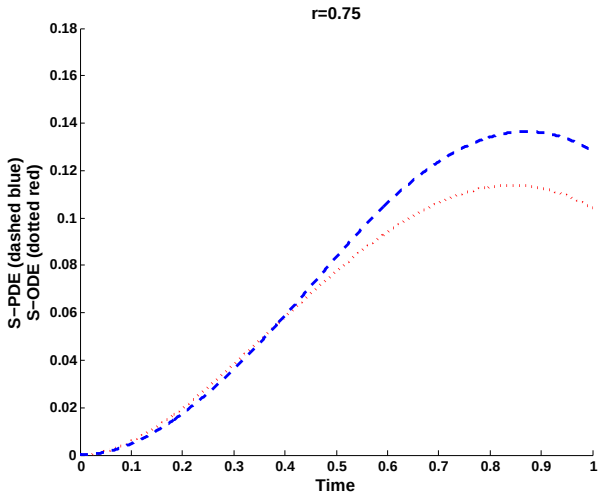


Figure 3.27: Comparison of ODE and PDE results for $r = 0.75$.

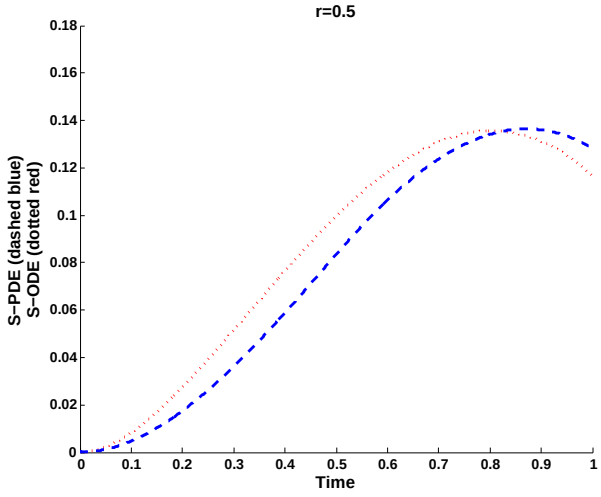


Figure 3.28: Comparison of ODE and PDE results for $r = 0.5$.

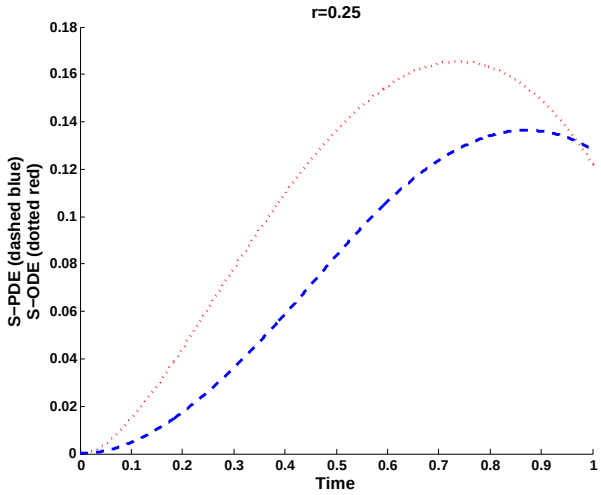


Figure 3.29: Comparison of ODE and PDE results for $r = 0.25$.

# Chapter 4

# Morales and Smith Simplification: Concerns and Alternate Approaches

As shown in Section 3.4, there is an inconsistency between the trajectories of the signal intensity, depending on how $S(t)$ is computed: numerically solving the PDE system (2.4) and integrating the results versus numerically solving the modified ODE system (2.12). The primary difference in these two systems of equations is the introduction of the Morales and Smith Simplification. This raises concerns regarding the validity of this simplification's applicability to this model. In Section 4.1, these concerns are discussed and verified using results from numerical simulations.

While the results shown in Section 4.1 challenge much of the research that has been done since the initial proposal of applying the Morales and Smith simplification to the two-compartment model almost a decade ago [4], the remainder of this chapter is dedicated to the development of alternative methods for recovering parameters. These alternative methods do not rely on the Morales and Smith Simplification. Section 4.2.1 presents a method for determining the perfusion coefficient, $F$, and computational results are provided. Section 4.2.2 explains how to recover the con-

centration of contrast agent leaving the capillary via the venule, $c_V(t)$, and provides results from numerical experiments. Section 4.2.3 describes how to determine the relative volume of the plasma compartment, $v_p$; computational results are provided. In an effort to capture the impact of data limitations due to the discrete nature of the medical imaging process, Section 4.3 provides results for the aforementioned methods using various downsampling rates of analytical baseline data. Section 4.4 summarizes the findings in this chapter.

## 4.1 Concerns Regarding the Validity of the Morales and Smith Simplification

Recall, Section 2.3 introduces the term, $c_V(t)$, that arises from the bounds of integration when reducing the system of PDEs (2.4) to the system to ODEs (2.7). Section 2.4 explains the difficulty involved in physically measuring this quantity. In an effort to eliminate this term from the equations, the Morales and Smith Simplification, (2.9), was proposed and implemented, resulting in the revised system of ODEs (2.12).

Historically, the relationship in (2.9) was developed to describe capillary reuptake under normal flow conditions [14]. In a steady state regime with no transport across the capillary wall, $c_A(t) = c_V(t) = \bar{c_p}(t) = K$, where $K$ is a constant, thus (2.9) holds trivially in this case. However, in more dynamic scenarios, this relationship may begin to break down. In dynamic imaging, the time scales are short, and concentration of contrast agent at any point in the system changes rather quickly in time. This raises a question as to the validity of the application of the Morales and Smith Simplification to the two-compartment model for the purposes of determining tumor blood flow parameters.

Using the two sets of baseline coefficients from Table 4.1 and the inflow boundary condition as defined in (2.25), $\bar{c_p}(t)$ and $c_V(t)$ are calculated at each time step.

Solving (2.9) for $r$,

$$r = \frac{c_A(t) - \bar{c_p}(t)}{c_A(t) - c_V(t)}. \tag{4.1}$$

By definition, $r$ should be a constant between 0 and 1, however, by computing the right hand side of (4.1), it is shown in Figures 4.1 and 4.2 that this assumption is not valid and that $r$ must be a function of time.

Table 4.1: Parameter values for two sets of baseline data.

| Data Set | $f$ | $P$ | $v_p$ | $v_e$ |
|---|---|---|---|---|
| A | 2.0 | 1.0 | 0.5 | 0.7 |
| B | 1.0 | 0.05 | 0.5 | 0.7 |

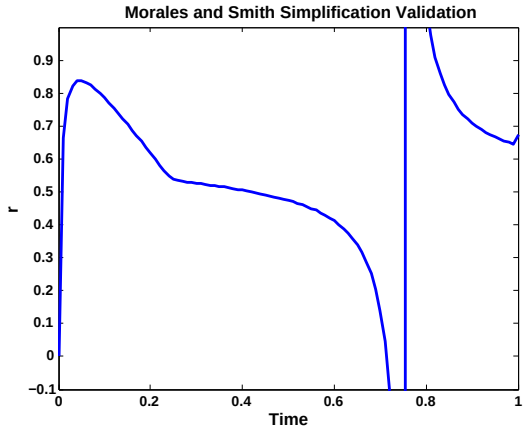


Figure 4.1: Plot of $r$ given by (4.1) for Model Data Set A.

The jumps in Figures 4.1 and 4.2 are a result of the singularity that occurs when $c_A = c_V$.

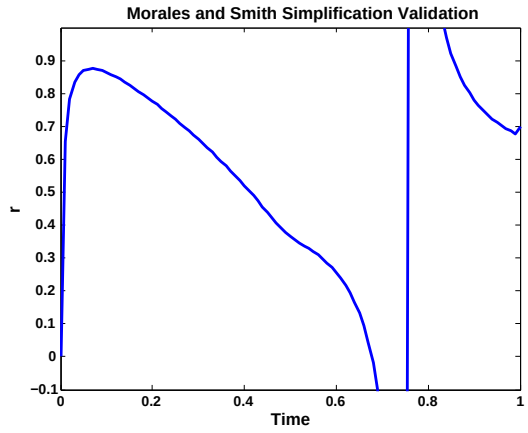


Figure 4.2: Plot of $r$ given by (4.1) for Model Data Set B.

## 4.2 New Methods without the Morales and Smith Simplification

As illustrated in Figures 4.1 and 4.2, the Morales and Smith simplification is not valid for this application. Therefore, the work described in this section uses the original system of ODEs (2.7) in lieu of those given by the simplified system of ODEs (2.12). This section describes methods for accurately calculating two of the four blood flow parameters, along with a method for determining $c_V(t)$. The presented results use data from the two model data sets, A and B. For each of the two data sets, a high fidelity set of analytical baseline data is calculated through numerically integrating the PDEs (2.3) and (2.2), using (2.25) as the inflow boundary condition and an initial condition of $c_p(x, t = 0) = c_e(x, t = 0) = 0$. Subsets of the resulting $c_A(t)$ and $S(t)$ analytical data representing $N$ equally spaced time steps of size $\Delta t$ are then passed into the algorithms described in the following subsections. This method of downsampling the analytical data is used to represent the discrete nature of the image capture process during an actual medical imaging test.

### 4.2.1 Recovering $F$

The perfusion coefficient, $F$, represents the flow rate of the contrast agent along the length of the capillary. This parameter is isolated through algebraic manipulations of the equations. First, (2.5) and (2.6) are added to get:

$$v_p \frac{\mathrm{d}\bar{c_p}(t)}{\mathrm{d}t} + v_e \frac{\mathrm{d}\bar{c_e}(t)}{\mathrm{d}t} = F(c_A(t) - c_V(t)), \tag{4.2}$$

where the left side is exactly equal to $\frac{\mathrm{d}S(t)}{\mathrm{d}t}$. Writing the left side as $S'(t)$ and solving (4.2) for $F$ results in:

$$F = \frac{S'(t)}{c_A(t) - c_V(t)}, \tag{4.3}$$

where $c_A(t)$ is known for each time step, and $S'(t)$ is calculated numerically for each time step using only the $N$ downsampled data points. Instead of using the Morales and Smith simplification to eliminate $c_V(t)$ from (4.3) [4, 13], it is assumed that $c_V(t) = 0$ for exactly the time it takes for the tracer to travel along the length of the capillary. While this time is not known a priori, (4.3) can be solved for $F$ by setting $c_V(t) = 0$ for all $t$. Plotting the resulting values of $F$ as a function of $t$, it is clear that the correct value can be extracted before the assumption of $c_V = 0$ becomes invalid. In theory, $F$ is simply the statistical mode of the results of (4.3), however, due to the number of digits maintained in the calculations, a simply computed mode is often an inaccurate choice for $F$. Thus, in practice, $F$ is recovered through binning the results from (4.3), and selecting the mean value of the most populated bin. Figures 4.3 and 4.4 show the results for Baseline Data Sets A and B respectively each with $\Delta t = 0.01$ and $T = 1$ ($N = 100$), and Table 4.2 shows the exact and calculated results for both data sets using downsampling rates for $\Delta t = 0.01$ ($N = 100$) and $\Delta t = 0.001$ ($N = 1000$), with $T = 1$ for both cases. Notice that in Figures 4.3 and 4.4, the value of $F$ computed using (4.3) quickly converges to the true value of $F$, but at some point, when the assumption of $c_V(t) = 0$ is no longer valid, the convergence is lost.

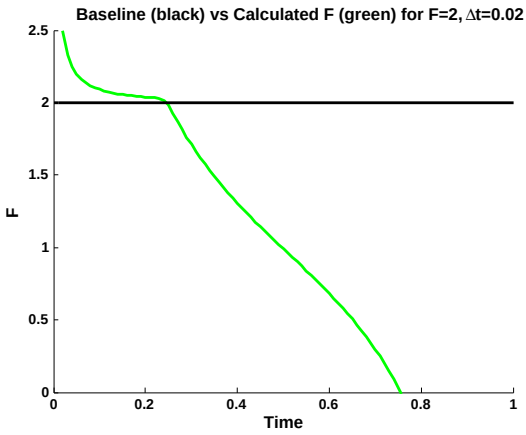


Figure 4.3: Plot of $F$ given by (4.3) for Model Data Set A. The horizontal line represents the actual value of $F$.

Table 4.2: Actual versus calculated values of $F$.

| Data Set | $\Delta t$ | $N$ | Actual $F$ | Calculated $F$ | %-error |
|---|---|---|---|---|---|
| A | 0.01 | 100 | 2.0 | 2.04 | 2.0% |
| A | 0.001 | 1000 | 2.0 | 2.01 | 0.5% |
| B | 0.01 | 100 | 1.0 | 1.01 | 1.0% |
| B | 0.001 | 1000 | 1.0 | 1.00 | 0.0% |

### 4.2.2 Recovering $c_V(t)$

Recall that the reason for invoking the Morales and Smith simplification was the difficulty of measuring $c_V(t)$ [4]. Instead, $c_V(t)$ can be directly calculated using the value of the constant, $F$, computed using the method described in the previous section. Solving (4.3) for $c_V(t)$ gives

$$c_V(t) = c_A(t) - \frac{S'(t)}{F}, \tag{4.4}$$

where the entire right hand side is known. Figures 4.5 and 4.6 show the comparison between the analytical data for $c_V(t)$ and the values calculated using (4.4) for Model Data Sets A and B, $\Delta t = 0.01$ and $T = 1$ ($N = 100$). In Figure 4.5, notice the

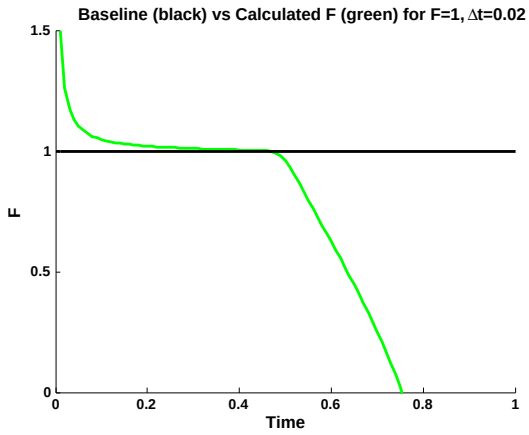


Figure 4.4: Plot of $F$ given by (4.3) for Model Data Set B. The horizontal line represents the actual value of $F$.

time when $c_V$ is no longer 0; this is the same time when the equation for $F$ began to breakdown in Figure 4.3. A similar result is seen in comparing the time when $c_V > 0$ in Figure 4.6 with the breakdown of (4.3) in Figure 4.4.

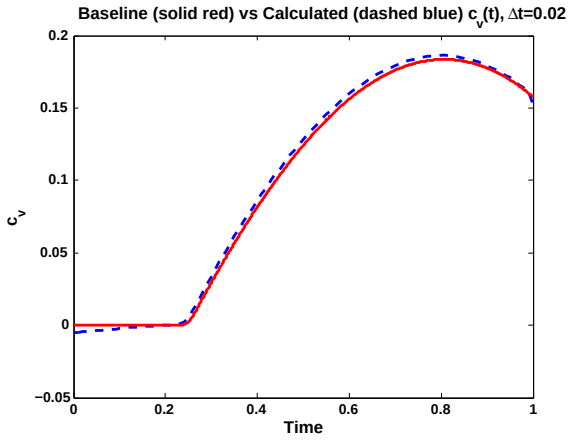


Figure 4.5: Plot of $c_V(t)$ given by (4.4) for Model Data Set A.

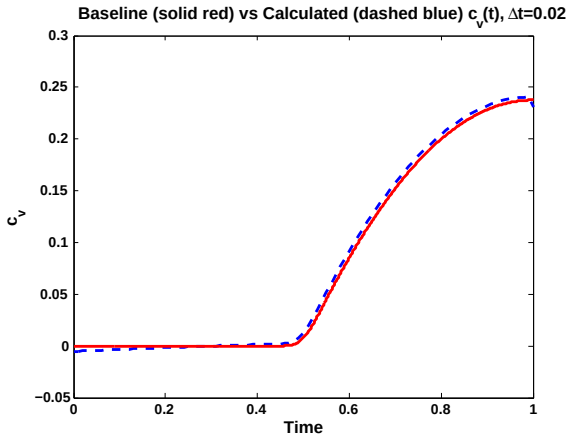


Figure 4.6: Plot of $c_V(t)$ given by (4.4) for Model Data Set B.

### 4.2.3 Recovering $v_p$

The first step to recovering the coefficient that represents volume of the plasma compartment is to determine the time, $t^*$, it takes for the contrast agent to travel along the length of the capillary and reach the venule. The value of $t^*$ is found by examining the calculated data for $c_V(t)$ to find the first time the data is greater than some threshold, $\epsilon$, greater than zero.

Dividing the original PDE (2.3) by $v_p$ and recalling that the problem is scaled to the length of the capillary, $L = 1$,

$$\frac{\partial c_p(x,t)}{\partial t} = -\frac{F}{v_p}\frac{\partial c_p(x,t)}{\partial x} - \frac{P}{v_p}\Big(c_p(x,t) - c_e(x,t)\Big), \tag{4.5}$$

where $\frac{F}{v_p}$ is the rate at which the contrast agent travels along the length of the capillary. Relating this rate, $\frac{F}{v_p}$, with the time, $t^*$, and again recalling $L = 1$,

$$v_p = Ft^*. \tag{4.6}$$

Table 4.3 presents the actual and calculated values of $t^*$ with the percent error for both Model Data Sets A and B, using $\Delta t = 0.01$ and $T = 1$ ($N = 100$). Table

4.4 gives the actual and calculated values of $v_p$ for these same cases. The results presented in Table 4.3 for both the actual and calculated values of $t^*$ were recovered using a threshold of $\epsilon = 0.005$.

Table 4.3: Actual versus calculated values of $t^*$.

| Data Set | Actual $t^*$ | Calculated $t^*$ | $t^*$-%-error |
|---|---|---|---|
| A | 0.2572 | 0.2500 | 2.80% |
| B | 0.4942 | 0.4900 | 0.85% |

Table 4.4: Actual versus calculated values of $v_p$.

| Data Set | Actual $v_p$ | Calculated $v_p$ | $v_p$-%-error |
|---|---|---|---|
| A | 0.5 | 0.5100 | 2.00% |
| B | 0.5 | 0.4949 | 1.02% |

## 4.3 Impact of Downsampling Rate on Accuracy

In Section 4.2.1, the coefficient, $F$, is recovered from a subset of analytical values for the signal intensity, $S(t)$. In Table 4.2, the results are shown for two cases, each with a different value of $\Delta t$, representing two different sampling rates. It is easy to predict that as $\Delta t$ increases, accuracy will decrease. At some point, there will simply not be enough data available to recover any parameters with any reasonable accuracy. By exploring the relationship between accuracy of recovered parameters and the sampling rate, the importance of image frequency can be better understood. In this section, the above methods for recovering $F$, $c_v(t)$, and $v_p$ are applied to Data Set B from Table 4.1 for various values of $\Delta t$. Figure 4.7 shows the signal intensity $S(t)$ and left boundary condition $c_A(t)$ for the full set of analytical data, $N = 5000$.

Tables 4.5 - 4.7 show the accuracy results for determining $F$, $t^*$ and $v_p$ for various values of $\Delta t$. It is clear from these results that these methods are robust up to a

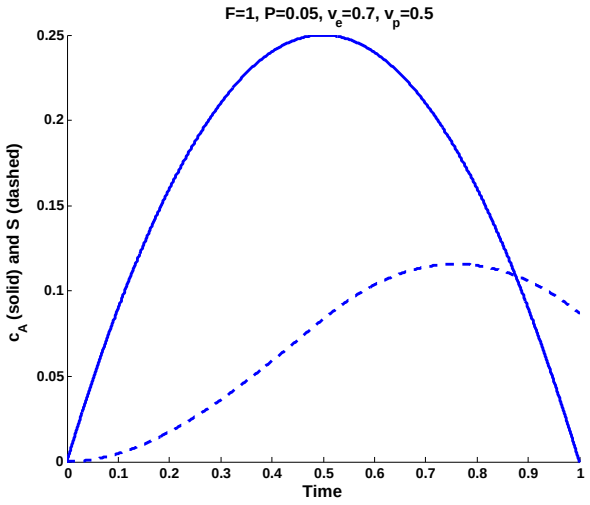


Figure 4.7: Analytical data for Data Set B.

point. However, if too little data is available, these methods will fail. While the results for $F$ in Table 4.5 look optimistic at $\Delta t = 0.04$, it should be noted that the confidence for this calculation of $F$ is very low as there are not many data points in any one bin. At $\Delta t = 0.1$, the method fails completely. The break-down process is illustrated in Figures 4.8 and 4.9.

Table 4.5: Actual versus calculated values of $F$ for varying $\Delta t$.

| $\Delta$t | $N$ | Actual $F$ | Calculated $F$ | %-error |
|---|---|---|---|---|
| 0.0002 | 5000 | 1.0 | 1.00 | 0.0% |
| 0.0004 | 2500 | 1.0 | 1.00 | 0.0% |
| 0.001 | 1000 | 1.0 | 1.00 | 0.0% |
| 0.002 | 500 | 1.0 | 1.00 | 0.0% |
| 0.004 | 250 | 1.0 | 1.00 | 0.0% |
| 0.01 | 100 | 1.0 | 1.01 | 1.0% |
| 0.02 | 50 | 1.0 | 1.01 | 1.0% |
| 0.04 | 25 | 1.0 | 1.01 | 1.0% |
| 0.1 | 10 | 1.0 | 0.04 | 96.0% |

In Figure 4.8, at a very high imaging frequency (low $\Delta t$), the value of $F$ calculated using (4.3) quickly converges to the actual value. Due to discontinuities at $t = 0$, it

Table 4.6: Actual versus calculated values of $t^*$ for varying $\Delta t$.

| $\Delta t$ | $N$ | Actual $t^*$ | Calculated $t^*$ | $t^*$-%-error |
|---|---|---|---|---|
| 0.0002 | 5000 | 0.4942 | 0.4942 | 0.00% |
| 0.0004 | 2500 | 0.4942 | 0.4936 | 0.12% |
| 0.001 | 1000 | 0.4942 | 0.4940 | 0.04% |
| 0.002 | 500 | 0.4942 | 0.4940 | 0.04% |
| 0.004 | 250 | 0.4942 | 0.4920 | 0.45% |
| 0.01 | 100 | 0.4942 | 0.4900 | 0.85% |
| 0.02 | 50 | 0.4942 | 0.4800 | 2.87% |
| 0.04 | 25 | 0.4942 | 0.4800 | 2.87% |
| 0.1 | 10 | 0.4942 | 0.8000 | 61.9% |

Table 4.7: Actual versus calculated values of $v_p$ for varying $\Delta t$.

| $\Delta t$ | $N$ | Actual $v_p$ | Calculated $v_p$ | $v_p$-%-error |
|---|---|---|---|---|
| 0.0002 | 5000 | 0.5 | 0.4942 | 1.16% |
| 0.0004 | 2500 | 0.5 | 0.4936 | 1.28% |
| 0.001 | 1000 | 0.5 | 0.4940 | 1.20% |
| 0.002 | 500 | 0.5 | 0.4940 | 1.20% |
| 0.004 | 250 | 0.5 | 0.4920 | 1.60% |
| 0.01 | 100 | 0.5 | 0.4949 | 1.02% |
| 0.02 | 50 | 0.5 | 0.4848 | 3.04% |
| 0.04 | 25 | 0.5 | 0.4848 | 3.04% |
| 0.1 | 10 | .5 | 0.0320 | 93.60% |

takes several timesteps for the solution of $F$ to converge. Naturally, as the imaging frequency is decreased, it takes more time to achieve the same convergence. Once the sampling rate is sufficiently low, there is simply not enough time for the solution to converge before the assumption that $c_V = 0$ is no longer relevant.

Though these methods fail in extreme cases when only a very small subset of the analytical data is available, the methods are quite robust for reasonable data sizes. Relating this back to the physical problem of medical imaging, this means that in the absence of noise these methods could be used with reasonable accuracy for even a relatively small number of images.

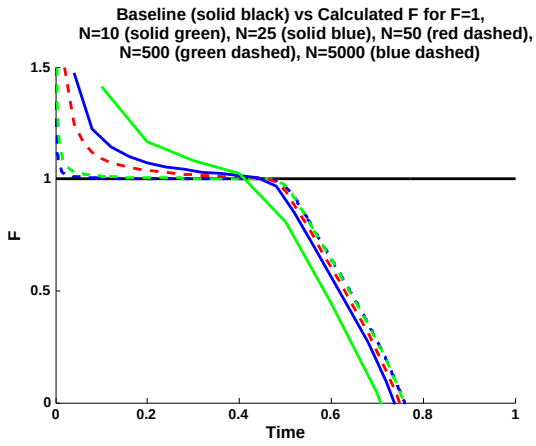


Figure 4.8: Plot of $F$ given by (4.3) for $\Delta t = \{0.01, 0.04, 0.02, 0.002, 0.0002\}$.

## 4.4 Summary

The initial purpose of the Morales and Smith assumption was to describe capillary reuptake under certain flow conditions. As shown in Section 4.1, this simplification does not hold in the application of contrast-enhanced medical imaging; the tunable parameter $r$ is demonstrated to be time-dependent while the simplification requires a constant value of $r$. The remainder of the chapter presented alternative methods for determining two of the coefficients, $F$ and $v_p$, and the outflow condition $c_v(t)$. These new methods are built based on the original ODE system (2.7) versus the simplified system (2.12) shown in Section 2.5. In addition to yeilding highly accurate results in the test cases in Sections 4.2.1-4.2.3, Section 4.3 showed that these methods provide promising results even at relatively low imaging frequencies.

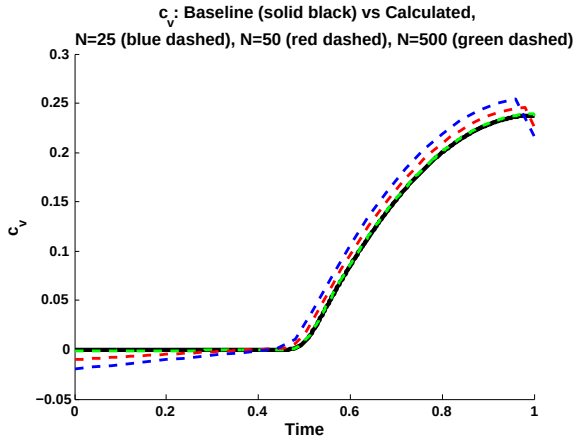


Figure 4.9: Plot of $c_V(t)$ given by (4.4) for $\Delta t = \{0.04, 0.02, 0.002\}$.

# Chapter 5

# Conclusion

## 5.1 Summary

Chapter 1 of this thesis presents the motivation for this research, provides a fundamental appreciation for the physiological phenomenology of angiogenesis, and explains the current common practices in measuring the efficacy of cancer treatments using medical imaging. Chapter 2 explains the relevant work in this field, and creates a foundation for the research presented in this thesis.

Building upon the first two chapters, Chapter 3 demonstrates the relationships between the signal intensity, $S(t)$, and the four coefficients of interest, $F$, $v_p$, $P$, and $v_e$. These relationships are explored through parametric studies using numerical experiments. Results arising from numerically solving the system of simplified ODEs (2.12) were compared with the results arising from numerically solving the system of PDEs (2.4). This comparison identified fundamental differences in these two systems of equations and led to an investigation of the underlying Morales and Smith Simplification and its applicability to this model in Chapter 4.

After showing that the Morales and Smith Simplification does not reproduce the correct physics in analytical results for the baseline problem, Chapter 4 goes on to present alternative methods for extracting some of the coefficients. The first coeffi-

cient recovered is the flow perfusion, $F$, then using this value of $F$, the right bound of integration, $c_v(t)$, can be directly computed. Finally, using these two pieces of information, the relative volume of the plasma compartment, $v_p$, is calculated. Through numerical experimentation, the accuracy of these methods are demonstrated. In these numerical experiments, values of $S(t)$ and $c_A(t)$ are downsampled from the analytical baseline dataset at even sampling rates to represent a sequence of images taken during an actual patient test scenario. As expected, there is a lower limit for the sampling rate, below which the data available is insufficient to accurately recover $F$, however, above this threshold, the methods presented prove to be fairly robust.

## 5.2 Ongoing and Future Work

Currently, there are three different directions in which this research is advancing. First, the methods described in Chapter 4 use evenly spaced downsampling from truth data. While this is representative of the discrete nature of the data collection process used in dynamic imaging techniques, it fails to capture the noise that is inherent in these patient tests. For this reason, the impact of applying random noise to the truth data is being studied. Once the robustness of the methods are measured, these methods will be tested against real patient data, and results will be compared against results obtained through the use of more traditional techniques.

The second direction for advancement involves recovering the two additional parameters: permeability surface area product, $P$, and the relative volume of the interstitial space, $v_e$. As one can notice in the parameter studies in Chapter 3, these two coefficients act together to impact the time of the maximum signal intensity. A trial and error method of adjusting these two coefficients and matching the position of this maximum point on the signal intensity curve, $S(t)$, has begun to show some useful results. In light of these discoveries, more work is now being done to extract these coefficients in a less rudimentary fashion.

The third direction is to continue collaboration with the radiology community. Currently, this work is being done in collaboration with researchers at L'Hôpital St. Louis and L'Hôpital European George Pompidou. Ultimately, the goal is to implement these methods in near real-time, such that this team of radiologists could access and use these methods on actual patients. Achieving this goal would reduce the time it takes to determine the efficacy of a cancer treatment on individual patients, thus decreasing time spent using ineffective treatments, minimizing unnecessary side effects, reducing treatment time and cost, and improving patient quality of care and quality of life.

# Bibliography


[1] Fung, *Biomechanics: Circulation, 2nd Edition*, Springer-Verlag New York, Inc., New York, 1997.

[2] D. Hanahan & R.A. Weinberg, *The hallmarks of cancer*, Cell 2000; **100**:57-70.

[3] G. Bergers & L.E. Benjamin, *Tumorigenesis and the angiogenic switch*, Nature Reviews: Cancer 2003; **3**:401-410.

[4] G. Brix et al., *Regional blood flow, capillary permeability, and compartmental volumes: measurement with dynamic CT — initial experience*, Radiology 1999; **210**:269-276.

[5] J.C. Miller et al., *Imaging angiogenesis: Applications and potential for drug development*, J Natl Cancer Inst. 2005; **97(3)**: 172 - 187.

[6] L.H.D. Cheong, C.C.T. Lim, & T.S. Koh, *Dynamic contrast-enhanced CT of intracranial meningioma: Comparison of distributed and compartmental tracer kinetic models–Initial results*, Radiology 2004; **232(3)**:921-930.

[7] A.F. DeVries et al., *Tumor microcirculation evaluated by dynamic magnetic resonance imaging predicts therapy outcome for primary rectal carcinoma*, Cancer Research 2001; **61(6)**:2513-2516.

[8] P. Liang et al., *Dynamic MRI signals in the second week of radiotherapy relate to treatment outcomes of hepatocellular carcinoma: a preliminary result*, Liver International 2007; **27(4)**:516-528.

[9] S. Vogel, *Vital Circuits*, Oxford University Press, Inc., New York, 1992.

[10] C.M. Zechmann et al., *Impact of stroma on the growth, microcirculation, and metabolism of experimental prostate tumors*, Neoplasia 2007; **9(1)**:57-67.

[11] G. Brix et al., *Microcirculation and microvasculature in breast tumors: Pharmacokinetic analysis of dynamic MR image series*, Magnetic Resonance in Medicine 2004; **52**:420429.

[12] T.S. Koh et al., *A physiologic model of capillary-tissue exchange for dynamic contrast-enhanced imaging of tumor microcirculation*, IEEE Trans. on Biomed Eng 2003; **v50.n2**.

[13] W.S. Don and D. Gottlieb, *Estimating kinetic parameters from MRI measurements of blood flow to tumors*, 6th Int. Conf. on Spectral and Higher Order Methods, Brown University, Providence, RI, USA, June 2004.

[14] M.F. Morales, R.E. Smith, *On the theory of blood-tissue exchange of inert gases. VI. Validity of approximate uptake expressions*, Bull Math Biophys 1948; **10**:191-200.